Frontiers in Bioscience Landmark

Front. Biosci. (Landmark Ed) **2026**; 31(9): 55796
https://doi.org/10.31083/FBL55796

Original Research

Commiphora africana Ethanol Extract Attenuates Inflammatory Responses With Reduced NF-κB/AP-1 Activation and Src/TAK1-Related Signaling Changes

Canglang Mou[1,†], Yuhao Wang[1,†], Lei Huang[2], Jinghan Su[1], Long You[3], Ziliang He[1], Yeye Hu[1], Weizhaole Wei[1], Wooram Choi[1], Byoung-Hee Lee[4], Woo Young Bang[4], Hye-Woo Byun[4], Jongsung Lee[1], Ji Hye Kim[1,*], Jae Youl Cho[1,2,*]

[1]Department of Integrative Biotechnology and Biomedical Institute for Convergence, Sungkyunkwan University, 16419 Suwon, Republic of Korea
[2]Department of Biocosmetics, Sungkyunkwan University, 16419 Suwon, Republic of Korea
[3]School of Life Sciences, Huaiyin Normal University, 223300 Huaian, Jiangsu, China
[4]Biological Resources Utilization Division, National Institute of Biological Resources, 22689 Incheon, Republic of Korea
*Correspondence: kjhkjhmlml@skku.edu (Ji Hye Kim); jaecho@skku.edu (Jae Youl Cho)
[†]These authors contributed equally.
Academic Editor: Shile Huang
Submitted: 9 July 2026 Revised: 20 August 2026 Accepted: 27 August 2026 Published: 20 September 2026

Abstract

Background: The bark, resin, and roots of *Commiphora africana* (A. Rich.) Engl. have traditionally been used in African medicine to treat fever, stomach disorders, colic, and swelling. However, despite this traditional use, its anti-inflammatory activity and the underlying molecular mechanisms remain poorly characterized. **Methods:** We evaluated the anti-inflammatory activity of *C. africana* ethanol extract (Caf-EE) in lipopolysaccharide (LPS)-stimulated macrophages and in murine models of HCl/EtOH-induced acute gastric mucosal injury and LPS-induced acute lung injury. Reporter assays, gene expression analysis, immunoblotting, cellular thermal shift assay (CETSA), gas chromatography–mass spectrometry (GC–MS)-guided compound annotation, network pharmacology, and molecular docking were used to investigate the anti-inflammatory mechanisms of Caf-EE. **Results:** Caf-EE inhibited nitrite production without cytotoxicity in LPS-stimulated RAW264.7 macrophages. GC–MS-guided feature annotation identified representative candidate constituents of Caf-EE, and network pharmacology indicated their association with inflammation-related pathways. Mechanistically, Caf-EE suppressed MyD88- and TRIF-mediated NF-κB/Activator protein 1 (AP-1) transcriptional activity and reduced the expression of inflammatory genes. Caf-EE also inhibited phosphorylation of Src/IκB kinase (IKK)/IκB- and Transforming growth factor-β-activated kinase 1 (TAK1)/c-Jun N-terminal kinase (JNK)/c-Jun-associated signaling proteins and increased the thermal stability of Src and TAK1. *In vivo*, Caf-EE attenuated HCl/EtOH-induced acute gastric mucosal injury and LPS-induced acute lung injury, accompanied by reduced phosphorylation of Src and TAK1 in both tissues. Among the representative GC–MS-annotated compounds, 9,19-cyclolanost-24-en-3-ol exhibited the highest predicted binding affinity for Src and TAK1 in molecular docking analysis. **Conclusions:** Collectively, this study provides mechanistic evidence for the anti-inflammatory effects of Caf-EE through modulation of Src/TAK1-associated signaling. Furthermore, the protective effects observed in acute inflammatory disease models support the further development of Caf-EE as a therapeutic candidate for inflammatory disorders.

Keywords: *Commiphora africana*; plant extracts; inflammation; signal transduction; protein kinases; acute lung injury; gastritis

1. Introduction

Inflammation is a protective response triggered by tissue injury, infection, or exposure to harmful endogenous or exogenous stimuli, including trauma, immune dysregulation, toxic chemicals, and microbial products [1,2]. In sentinel antigen-presenting cells (APCs), pattern-recognition receptors (PRRs) detect pathogen-associated molecular patterns (PAMPs) and initiate innate immune signaling, thereby promoting the recruitment of immune cells and shaping subsequent adaptive immune responses [3,4,5].

Among PRRs, Toll-like receptors (TLRs) are central regulators of inflammatory signaling. Different TLRs recognize distinct microbial ligands, including lipopolysaccharide (LPS; TLR4), bacterial lipoproteins (TLR2), and flagellin (TLR5) [6]. In the present study, we focused primarily on the TLR4-relevant inflammatory context. Upon recognition of LPS by the TLR4-MD2 complex, TLR4 activates both the MyD88-Mal and TIR-domain-containing adapter-inducing interferon-β (TRIF)-TRIF-related adaptor molecule (TRAM) adaptor pathways [6,7,8]. These convergent signaling cascades subsequently activate IκB kinase (IKK)/NF-κB and MAPK/Activator protein 1 (AP-1) pathways, leading to the transcription of pro-inflammatory mediators [9,10,11]. Within this network, Src functions as a critical upstream regulator of NF-κB activation, while Transforming growth factor-β-activated kinase 1 (TAK1) serves as a central signaling hub linking TLR4 activation to

both NF-κB and MAPK/AP-1 pathways [12,13,14]. Given that the dysregulation of this network contributes to various inflammatory diseases, modulating these pathways represents a viable strategy for anti-inflammatory intervention.

Although aspirin and other nonsteroidal anti-inflammatory drugs (NSAIDs) suppress inflammation in part through cyclooxygenase/prostaglandin-related mechanisms [15,16], their long-term clinical use is constrained by adverse effects, particularly gastrointestinal injury [17]. Accordingly, there is sustained interest in identifying safer anti-inflammatory agents derived from medicinal plants with a history of traditional use.

The genus *Commiphora* (Burseraceae) comprises over 200 species distributed across Africa, the Middle East, and parts of Asia. Extracts and oleo-gum resins from *Commiphora* species are known to possess diverse pharmacological properties, including anti-inflammatory, antimicrobial, antioxidant, and anticancer activities [18]. A representative species, *Commiphora africana* (A. Rich.) Engl., commonly known as African myrrh, is a small deciduous tree widely distributed across sub-Saharan Africa. In traditional African medicine, its bark, resin, and roots have been used to treat fever, stomach disorders, colic, swelling, malaria, leprosy, and various poisoning conditions. Previous studies have demonstrated antimalarial, antitumor, and antivenom activities of *C. africana* [19,20,21]. However, despite its traditional use for inflammatory disorders, the anti-inflammatory activity of *C. africana* and its underlying molecular mechanisms remain poorly characterized.

In the present study, we investigated the anti-inflammatory activity of *C. africana* ethanol extract (Caf-EE) in LPS-stimulated macrophages and murine models of acute gastric mucosal injury and acute lung injury. To elucidate the underlying mechanisms, we integrated network pharmacology with signaling analyses, cellular thermal shift assay (CETSA), and molecular docking, with particular emphasis on Src/TAK1-associated signaling.

2. Materials and Methods

2.1 Materials

Caf-EE (batch number: NIBR-1225) was supplied by the National Institute of Biological Resources (Incheon, Republic of Korea). RAW 264.7 and HEK293T cell lines were obtained from Cytion (Cat. No. 400319, Heidelberg, Germany) and the American Type Culture Collection (ATCC, Cat. No. CRL-3216, Manassas, VA, USA), respectively. Cell-line identity was verified by supplier-provided short tandem repeat (STR) profiling. All cell lines were routinely tested for mycoplasma contamination and confirmed to be negative. Culture media (RPMI-1640, DMEM) and Opti-MEM were from Gibco (Thermo Fisher Scientific, Waltham, MA, USA). Small-molecule reagents—including MTT, polyethylenimine (PEI), DMSO, LPS, ranitidine, prednisolone, and dexamethasone—were sourced from Sigma-Aldrich (St. Louis, MO, USA). We used a Thermo Fisher Scientific cDNA kit, Macrogen-synthesized primers for RT-PCR, and PCR premix from Bio-D (Seoul, Republic of Korea). Chemiluminescent detection reagents for immunoblotting were obtained from ATTO (Tokyo, Japan). The primary antibodies used for immunoblotting included p-NF-κB p65 (Ser468; Cat. No. 3039), NF-κB p65 (Cat. No. 8242), NF-κB1 p105/p50 (Cat. No. 12540), p-IκBα (Cat. No. 9246), IκBα (Cat. No. 9242), p-IKKα/β (Cat. No. 2697), IKKα (Cat. No. 2682), p-Src (Tyr416; Cat. No. 2101), Src (Cat. No. 2109), p-c-Jun (Ser73; Cat. No. 9164), c-Jun (Cat. No. 9165), p-MKK7 (Cat. No. 4171), MKK7 (Cat. No. 4172), p-MKK4 (Cat. No. 9151), MKK4 (Cat. No. 9152), p-TAK1 (Ser412; Cat. No. 9339), TAK1 (Cat. No. 4505), p-p38 MAPK (Cat. No. 4631), p38 MAPK (Cat. No. 9212), p-SAPK/JNK (Cat. No. 9255), JNK2 (Cat. No. 4672), and HA-tag (Cat. No. 2367), which were purchased from Cell Signaling Technology (Danvers, MA, USA). p-NF-κB p50 (Ser337; Cat. No. sc-271908) and β-actin (Cat. No. sc-47778) were obtained from Santa Cruz Biotechnology (Dallas, TX, USA). HRP-conjugated goat anti-rabbit IgG (Cat. No. 7074) and goat anti-mouse IgG (Cat. No. 7076) secondary antibodies were obtained from Cell Signaling Technology (Danvers, MA, USA). Primary and secondary antibodies were diluted 1:2500 (2 µL per 5 mL of antibody diluent). Unless stated otherwise, all reagents were used as received and handled according to the manufacturers' instructions.

2.2 Cell Culture

RAW264.7 cells were cultured in RPMI-1640 and HEK293T in DMEM under standard conditions (37 °C, 5% CO_2, humidified). Cells at passages 3–10 were used for all experiments.

2.3 Extract Processing and Gas Chromatography-Mass Spectrometry

Leaves of *C. africana* were provided by the Wildlife Natural Products Bank at the National Institute of Biological Resources (NIBR), Incheon, Republic of Korea. Taxonomic identification and authentication of the plant material were performed by NIBR. An officially designated voucher specimen (No. NIBR202307203) was deposited in the herbarium of the NIBR repository.

For extract preparation, the air-dried leaves of *C. africana* (1.08 kg) were finely pulverized and extracted with 70% (v/v) ethanol at a solid-to-solvent ratio of 1:16.7 (w/v) using ultrasonic cleaners (UC-10 and UC-20, 400 W) at 50 °C for 3 h. The extraction was repeated three times, using 18 L of 70% ethanol for each extraction cycle. The combined extracts were filtered and concentrated under reduced pressure at 40 °C using a rotary evaporator (Büchi AG, Flawil, Switzerland), followed by lyophilization at –80 °C for 48 h. The extraction yield was 14.11%, and the resulting extract was designated Caf-EE.

The phytochemical profile of Caf-EE was examined by gas chromatography–mass spectrometry (GC–MS) with support from the Cooperative Center for Research Facilities at Sungkyunkwan University (Suwon, Republic of Korea), following previously established procedures [22]. GC–MS library matching was used to generate a tentative feature list. Representative lanostane-, cyclolanostane-, and triterpenoid-like annotations with relatively high library match quality and/or prominent relative peak areas were prioritized for extract-level downstream hypothesis generation. Because authentic standards and orthogonal chromatographic confirmation were not available, all entries were interpreted as tentative GC–MS features rather than confirmed constituents. The complete tentative feature list is provided in **Supplementary Table 1**.

2.4 Animals and Study Approval

Male ICR and C57BL/6J mice (6 weeks old; Orient Bio, Seongnam, Republic of Korea) were housed at five animals per cage under standard conditions with free access to food and water. A total of 73 mice were used in this study: 35 ICR mice for the HCl/EtOH-induced gastric mucosal injury experiment, 35 C57BL/6J mice for the LPS-induced acute lung injury experiment, and three C57BL/6J mice for primary peritoneal macrophage isolation.

After 5 days of acclimatization, mice used in each *in vivo* model were randomly allocated to five experimental groups (n = 7 per group). Each individual mouse was considered an independent experimental unit for the *in vivo* analyses. Sample sizes of seven mice per group were selected based on our previous experience with these acute inflammation models and prior studies [23,24] using comparable endpoints; no formal a priori sample-size calculation was performed. No a priori data-exclusion criteria were specified beyond the protocol-defined humane endpoints, and no animals, experimental units, or data points were excluded from the reported analyses.

Personnel administering the treatments were unaware of group allocation. Molecular experiments, including RT-PCR and immunoblotting, were performed using uncoded samples and were therefore not conducted under blinded conditions. However, outcome quantification, densitometric analysis, and statistical analysis were performed by investigators unaware of group allocation.

To minimize potential confounding, animals were maintained under the same housing conditions, and treatment administration and tissue collection were conducted according to predefined schedules across groups. Animals were monitored throughout the experiments for general condition and signs of distress in accordance with the approved animal protocol, and humane endpoints were applied when necessary.

All animal procedures were approved by the Institutional Animal Care and Use Committee of Sungkyunkwan University (protocol no. SKKUIACUC2024-07-02-1) and were performed in accordance with institutional guidelines for the care and use of laboratory animals. This study is reported in accordance with the ARRIVE 2.0 guidelines.

2.5 Target Prediction and Network Analysis

Six representative tentative GC–MS features, including Peak 25 (Lanosta-8,24-dien-3-one), Peak 26 (Lanost-8-en-7-one), Peak 33 (9,19-Cyclolanost-24-en-3-ol), Peak 35 (Glutinol), Peak 38 (9,19-Cyclolanostan-3-ol, 24-methylene-, (3β)-), and Peak 41 (Lanost-8-ene-3,7-dione), were submitted to SwissTargetPrediction (https://www.swisstargetprediction.ch/) [25] with the species restricted to Homo sapiens. Target symbols were standardized to human gene symbols, entries without a usable gene symbol were excluded, and duplicates were removed, yielding 195 unique putative targets. Gastritis-associated and bacterial-pneumonia-associated gene sets were obtained from the DISEASES text-mining resource through Harmonizome [26,27] and combined as a gastric/pulmonary inflammation-oriented disease set; removal of duplicate symbols yielded 951 genes. Intersection of the 195 putative targets with the 951 disease-associated genes identified 55 overlapping genes. A protein–protein interaction network was generated in STRING (https://string-db.org/) [28] using a minimum required interaction score of 0.700 and visualized in Cytoscape v3.10.1 (https://cytoscape.org/) [29]. Node degree was defined as the number of edges incident to each node and was calculated using Cytoscape NetworkAnalyzer. Gene Ontology (GO) biological-process and Kyoto Encyclopedia of Genes and Genomes (KEGG) pathway enrichment analyses used the 55 overlap genes as input in STRING for Homo sapiens; terms with a false discovery rate (FDR)-adjusted p value < 0.05 were retained.

2.6 Molecular Docking Analysis

For the main docking analysis, the crystal structures of human c-Src (PDB 2SRC) and TAK1/MAP3K7 (PDB 5V5N) were obtained from the Research Collaboratory for Structural Bioinformatics (RCSB) Protein Data Bank (https://www.rcsb.org/). Chain A residues 251–533 of 2SRC and residues 27–303 of 5V5N were retained using original PDB numbering. Waters and co-crystallized ligands were removed, polar hydrogens were added, and Gasteiger charges were assigned using AutoDockTools. Docking grids were centered on the co-crystallized adenylyl-imidodiphosphate (AMP-PNP) and takinib pockets, respectively. Four representative tentative GC–MS features were prepared from PubChem-derived three-dimensional structures, protonated, minimized with Merck Molecular Force Field 94 (MMFF94), and converted to Protein Data Bank, Partial Charge (Q), and Atom Type (T) (PDBQT) format. AutoDock Vina 1.2.7 (https://autodocksuite.scripps.edu/) [30] was run with exhaustiveness 16, nine output modes, an energy range of 3 kcal/mol, and random seed 20260703. The lowest-energy pose within each predefined kinase pocket was retained.

To validate the docking protocol, the co-crystallized ligands AMP-PNP (ANP) and takinib (EDH) were re-docked into the binding pockets of Src and TAK1, respectively. Redocking was performed using the same receptor and ligand preparation procedures, docking grids, and Vina parameters as those used for the main docking analysis. The redocked poses were compared with their corresponding crystallographic poses using heavy-atom root-mean-square deviation (RMSD). Both atom-name-mapped heavy-atom RMSD and symmetry-corrected heavy-atom RMSD calculated using RDKit GetBestRMS (https://www.rdkit.org/) were evaluated, with an RMSD of ≤2.0 Å considered indicative of successful reproduction of the crystallographic binding pose.

2.7 Cell Viability Assay

Cells were seeded at 1×10^5 cells/well in 96-well plates and equilibrated for 16–18 h. After 24 h of Caf-EE treatment, MTT solution (5 mg/mL; 10 µL/well) was added, and cells were incubated for 3–4 h at 37 °C. Formazan was dissolved overnight in 10% SDS/1 M HCl (100 µL/well). Absorbance was measured at 570 nm after subtraction of medium blanks.

2.8 Peritoneal Macrophage Isolation

A total of three male C57BL/6J mice aged 6 weeks were used for peritoneal macrophage isolation. Mice were administered 1 mL of 4% thioglycolate by intraperitoneal injection to stimulate macrophage recruitment. After 96 h, peritoneal lavage was performed to collect the cells. The identity of the isolated primary peritoneal macrophages was confirmed by flow cytometric analysis of the macrophage surface markers F4/80 and CD11b. Preparations containing >80% $F4/80^+CD11b^+$ cells were used for subsequent experiments. The isolated primary peritoneal macrophages were also tested for mycoplasma contamination and confirmed to be negative.

2.9 Nitric Oxide Assay

RAW264.7 cells and primary peritoneal macrophages were seeded in 96-well plates and equilibrated for approximately 20 h. Cells were pretreated with Caf-EE or prednisolone for 30 min and then stimulated with LPS for 24 h. Prednisolone served as the positive control for the macrophage nitrite assay. Nitrite accumulation in the culture supernatant was measured using the Griess reaction. Briefly, 100 µL of culture supernatant was mixed with an equal volume of Griess reagent, incubated for 5–10 min at room temperature, and measured at 540 nm.

2.10 RT-PCR for Gene Expression

Following Caf-EE pretreatment (30 min), RAW264.7 cells underwent 6 h LPS stimulation. Stomach and lung samples were milled under liquid nitrogen. RNA was then isolated from cells and tissues using 300 µL and 800 µL of TRIzol (Thermo Fisher Scientific, Waltham, MA, USA). From 1 µg RNA, cDNA was synthesized, and inflammatory transcripts, including inducible nitric oxide synthase (iNOS), IL-1β, IL-6, TNF-α, and GAPDH, were analyzed by semi-quantitative RT-PCR as indicated in each experiment (primer sequences in Table 1).

2.11 Luciferase Reporter Assays

HEK293T cells were PEI-transfected (MyD88 or TRIF; NF-κB-Luc/AP-1-Luc; β-gal) after overnight seeding (2.5×10^5 per well, 24-well). Caf-EE (50/75/100 µg/mL) was added 24 h later for 24 h, and firefly signals were normalized to β-gal activity.

2.12 HCl/EtOH-Induced Acute Gastric Mucosal Injury Model

Following our prior protocol [31], male ICR mice were randomized (n = 7/group) and orally administered vehicle (0.5% carboxymethyl cellulose [CMC]), Caf-EE (50 or 100 mg/kg), or ranitidine (40 mg/kg; positive control) twice daily for 2 consecutive days (four administrations). Treatments were administered at 0, 12, 24, and 36 h. Caf-EE was suspended in 0.5% CMC at concentrations of 5 and 10 mg/mL, and ranitidine was prepared at 4 mg/mL. Oral administration volumes were adjusted according to individual body weight to achieve the indicated doses, corresponding to 200 µL for a 20-g mouse.

Food was withdrawn beginning at 20 h and withheld for 24 h before induction of gastric injury. At 44 h, acute gastric mucosal injury was induced by oral administration of 300 µL of freshly prepared 200 mM HCl in 60% ethanol. One hour later (45 h), mice were euthanized using the open-drop isoflurane method in a closed chamber. Isoflurane (100%) was applied to absorbent material at 0.15 mL per liter of chamber volume, corresponding to an estimated nominal chamber concentration of approximately 3%. The absorbent material was physically separated from the animals to prevent direct contact with the liquid anesthetic. A deep plane of anesthesia was confirmed by the absence of the pedal withdrawal reflex in response to a firm toe pinch and the absence of the corneal reflex. The mice remained in the chamber until respiratory arrest was observed, after which cervical dislocation was performed as a secondary physical method to ensure irreversible death, and stomach tissues were collected for subsequent analyses. Because this model is based on a single acute chemical challenge followed by tissue evaluation 1 h later, the pretreatment dosing schedule was selected to evaluate the effect of Caf-EE against acute gastric mucosal injury.

Gastric lesion area was quantified using ImageJ v1.43r software (National Institutes of Health, Bethesda, MD, USA). Outcome measures included gastric lesion area, gastric Il1b and Il6 expression, and Src/TAK1-related phosphorylation signals in stomach tissue. Gastric lesion quantification was performed by an investigator blinded to group allocation.

Table 1. Primers used for semi-quantitative RT-PCR.

Gene	Forward primer (5′–3′)	Reverse primer (5′–3′)
iNOS	GGAGCCTTTAGACCTCAACAGA	TGAACGAGGAGGGTGGTG
IL-1β	CAGGATGAGGACATGAGCACC	CTCTGCAGACTCAAACTCCAC
IL-6	TACCCCCAGGAGAAGATTCC	TTTTCTGCCAGTGCCTCTTT
TNF-α	TTGACCTCAGCGCTGAGTTG	CCTGTAGCCCACGTCGTAGC
GAPDH	GCACCGTCAAGGCTGAGAAC	ATGGTGGTGAAGACGCCAGT

RT-PCR, reverse transcription polymerase chain reaction.

2.13 LPS-Induced Acute Lung Injury Model

Following a previously published protocol [31], male C57BL/6J mice (6 weeks old) were randomly allocated into five groups (n = 7 per group). Mice were orally administered vehicle (PBS), Caf-EE (50 or 100 mg/kg), or dexamethasone (5 mg/kg; positive control) at 0, 6, and 9 h. Caf-EE was prepared in PBS at concentrations of 5 and 10 mg/mL, and dexamethasone was prepared at 0.5 mg/mL. Oral administration volumes were adjusted according to individual body weight to achieve the indicated doses, corresponding to 200 µL for a 20-g mouse.

Acute lung injury was induced by intranasal administration of LPS (10 mg/kg) at 7 and 8 h; control mice received an equal volume of sterile PBS. LPS was freshly prepared in sterile PBS at 4 mg/mL and administered intranasally at 10 mg/kg. The intranasal administration volume was adjusted according to individual body weight, corresponding to 50 µL for a 20-g mouse. Each intranasal administration was delivered in multiple small aliquots to minimize distress, as described previously. Because this model involves two consecutive LPS challenges followed by tissue collection 16 h after the second LPS administration, the experimental design enabled assessment of the anti-inflammatory activity of Caf-EE under both pre- and post-LPS challenge conditions. Accordingly, repeated oral administration before and after LPS challenge was adopted.

At 24 h, mice were euthanized using the open-drop isoflurane method in a closed chamber. Isoflurane (100%) was applied to absorbent material at 0.15 mL per liter of chamber volume, corresponding to an estimated nominal chamber concentration of approximately 3%. The absorbent material was physically separated from the animals to prevent direct contact with the liquid anesthetic. A deep plane of anesthesia was confirmed by the absence of the pedal withdrawal reflex in response to a firm toe pinch and the absence of the corneal reflex. The mice remained in the chamber until respiratory arrest was observed, after which cervical dislocation was performed as a secondary physical method to ensure irreversible death. This time point corresponded to 16 h after the second LPS administration and 15 h after the final oral treatment. Lung tissues were collected for histological assessment, wet-to-dry ratio analysis, RT-PCR, and immunoblotting. Outcome measures included lung histology, lung wet-to-dry ratio, pulmonary inflammatory gene expression, and Src/TAK1-related phosphorylation signals. Histological assessment was performed by an assessor blinded to group allocation.

2.14 Protein Extraction and Immunoblot Analysis

After treatment, RAW264.7 and HEK293T cultures were lysed on ice in lysis buffer; lung and stomach tissues from the *in vivo* experiments were processed similarly. Proteins were analyzed by SDS-PAGE and immunoblotting using standard procedures.

2.15 Quantification of Lung Edema

Left lung lobes (n = 7 per group) were excised, rinsed in PBS, gently blotted to remove surface fluid, and weighed immediately (wet weight). After wet weighing, lungs were dried in a ventilated oven (80 °C, 72 h) and reweighed; edema was quantified as W/D, calculated as wet weight divided by dry weight [22].

2.16 Histological Analysis of Lung Tissue

Formalin-fixed (4% neutral buffered formalin [NBF], 48 h), paraffin-embedded lung tissues were sectioned (4 µm) and stained with H&E. Histologic injury was assessed blindly using a standardized scale encompassing septal thickening, alveolar/interstitial neutrophils, and hyaline membranes/proteinaceous material [22,31].

2.17 ATP-Dependent Src Autophosphorylation Assay

HEK293T cells expressing empty vector or HA-Src were harvested after transfection, and HA-Src-containing lysates were immunoprecipitated using an anti-HA antibody. After washing, the immunoprecipitates were incubated in kinase reaction buffer containing 25 mM Tris-HCl (pH 7.5), 5 mM β-glycerophosphate, 2 mM dithiothreitol, 0.1 mM sodium orthovanadate, and 10 mM $MgCl_2$. Vehicle, Caf-EE (100 µg/mL), or PP2 (20 µM) was added as indicated, and the autophosphorylation reaction was initiated by adding ATP to a final concentration of 200 µM. Empty-vector immunoprecipitates incubated with ATP and HA-Src immunoprecipitates incubated without ATP were included as negative controls. Reactions were conducted at 30 °C for 20 min and terminated by adding SDS sample buffer followed by boiling. Src Tyr416 phosphorylation and immunoprecipitated HA-Src were assessed by immunoblotting. Src autophosphorylation was quantified as the p-Src

Tyr416/HA-Src densitometric ratio and normalized to the mean of the HA-Src + ATP + vehicle group, which was set to 1.

2.18 Cellular Thermal Shift Assay

For CETSA, HEK293T cells expressing HA-tagged Src or HA-tagged TAK1 were treated with DMSO or Caf-EE (100 µg/mL). Preliminary temperature-range screening was performed before the formal CETSA experiments to determine the temperature ranges over which changes in soluble Src and TAK1 protein levels were observed. Based on these preliminary results, HA-Src samples were analyzed across 50–80 °C, whereas HA-TAK1 samples were analyzed across 40–50 °C. After heating, samples were cooled, lysed, clarified, and the soluble protein fractions were analyzed by immunoblotting according to established CETSA protocols [32,33].

2.19 Statistical Analysis

Quantitative data are presented as mean ± SD. For *in vitro* experiments, data represent three biologically independent experiments unless otherwise indicated. For nitric oxide, cell viability, and luciferase reporter assays, statistical significance was assessed using one-way ANOVA followed by Tukey's multiple-comparisons test. For semi-quantitative RT-PCR quantification, target/GAPDH ratios were calculated for each biological replicate and normalized to the LPS-treated group. Two separate one-way ANOVA analyses followed by Dunnett's multiple-comparisons test were performed: one comparing the LPS-treated group with the unstimulated control group and the other comparing each Caf-EE-treated group with the LPS-treated group. For time-course immunoblot analyses, LPS-stimulated groups were compared with the unstimulated control using one-way ANOVA followed by Dunnett's multiple-comparisons test, whereas LPS + Caf-EE groups were compared with the time-matched LPS groups using two-way ANOVA followed by Šídák-adjusted multiple comparisons. For immunoblot analysis of Src phosphorylation in HA-Src-overexpressing cells, statistical significance was assessed using one-way ANOVA followed by Dunnett's multiple-comparisons test. ATP-dependent Src autophosphorylation data were analyzed using repeated-measures one-way ANOVA followed by Dunnett's multiple-comparisons test.

For *in vivo* experiments, the experimental unit was one mouse, with seven mice per group. For tissue-based RT-PCR and immunoblot analyses, three randomly selected mice per group were used for the quantitative analyses. For all *in vivo* data, two separate one-way ANOVA analyses followed by Dunnett's multiple-comparisons test were performed: one comparing the HCl/EtOH- or LPS-treated group with the corresponding control group and the other comparing each treatment group with the HCl/EtOH- or LPS-treated group. Given the small sample sizes, formal assessment of distributional assumptions was not performed.

Statistical analyses were performed using GraphPad Prism 8.01 (GraphPad Software; https://www.graphpad.com/), and $p < 0.05$ was considered statistically significant.

3. Results

3.1 Anti-Inflammatory Activity and GC–MS Profile of Caf-EE

To evaluate the anti-inflammatory activity of Caf-EE, nitrite production was measured in LPS-stimulated macrophages. LPS (1 µg/mL) markedly increased nitrite production, whereas Caf-EE reduced it to less than 20% of the LPS control at 75 and 100 µg/mL (Fig. 1A). Caf-EE did not affect the viability of RAW264.7 or HEK293T cells after 24 h of treatment (Fig. 1B,C). Prednisolone, used as a positive control, significantly decreased the LPS-induced nitrite response (Fig. 1D). In primary mouse macrophages, Caf-EE likewise suppressed LPS-induced nitrite accumulation without cytotoxicity (Fig. 1E,F). Notably, LPS alone reduced the viability of primary macrophages by approximately 60%, whereas co-treatment with Caf-EE mitigated this cytotoxicity, increasing viability by 15% and 23% at 50 and 100 µg/mL, respectively (Fig. 1G). Overall, Caf-EE markedly attenuated production of nitrite in macrophages while preserving, and in primary cells even improving, cell viability.

GC–MS library matching tentatively annotated several lanostane- and cycloartane-type triterpenoid-related features in Caf-EE (Fig. 1H; Table 2). An enlarged 27.5–33.0 min region containing the six representative tentative features is shown in Fig. 1H, whereas the complete full-range total-ion chromatogram is provided in **Supplementary Fig. 1**. These features were subsequently used for exploratory downstream computational analyses, as specified in Table 2. The complete annotation list is provided in **Supplementary Table 1**.

3.2 Network Pharmacology Analysis Supporting the Anti-Inflammatory Activity of Caf-EE

Target prediction of representative tentative GC–MS features of Caf-EE yielded 195 unique putative targets. Intersection of these predicted targets with 951 gastric and pulmonary inflammation-associated genes identified 55 overlapping targets (Fig. 2A). STRING protein–protein interaction analysis identified tumor necrosis factor (TNF), interleukin 6 (IL6), AKT serine/threonine kinase 1 (AKT1), epidermal growth factor receptor (EGFR), heat shock protein 90 alpha family class A member 1 (HSP90AA1), Jun proto-oncogene, AP-1 transcription factor subunit (JUN), mitogen-activated protein kinase 3 (MAPK3), hypoxia-inducible factor 1 subunit alpha (HIF1A), prostaglandin-endoperoxide synthase 2 (PTGS2), and Janus kinase 2 (JAK2) as major hub proteins within the overlapping tar-

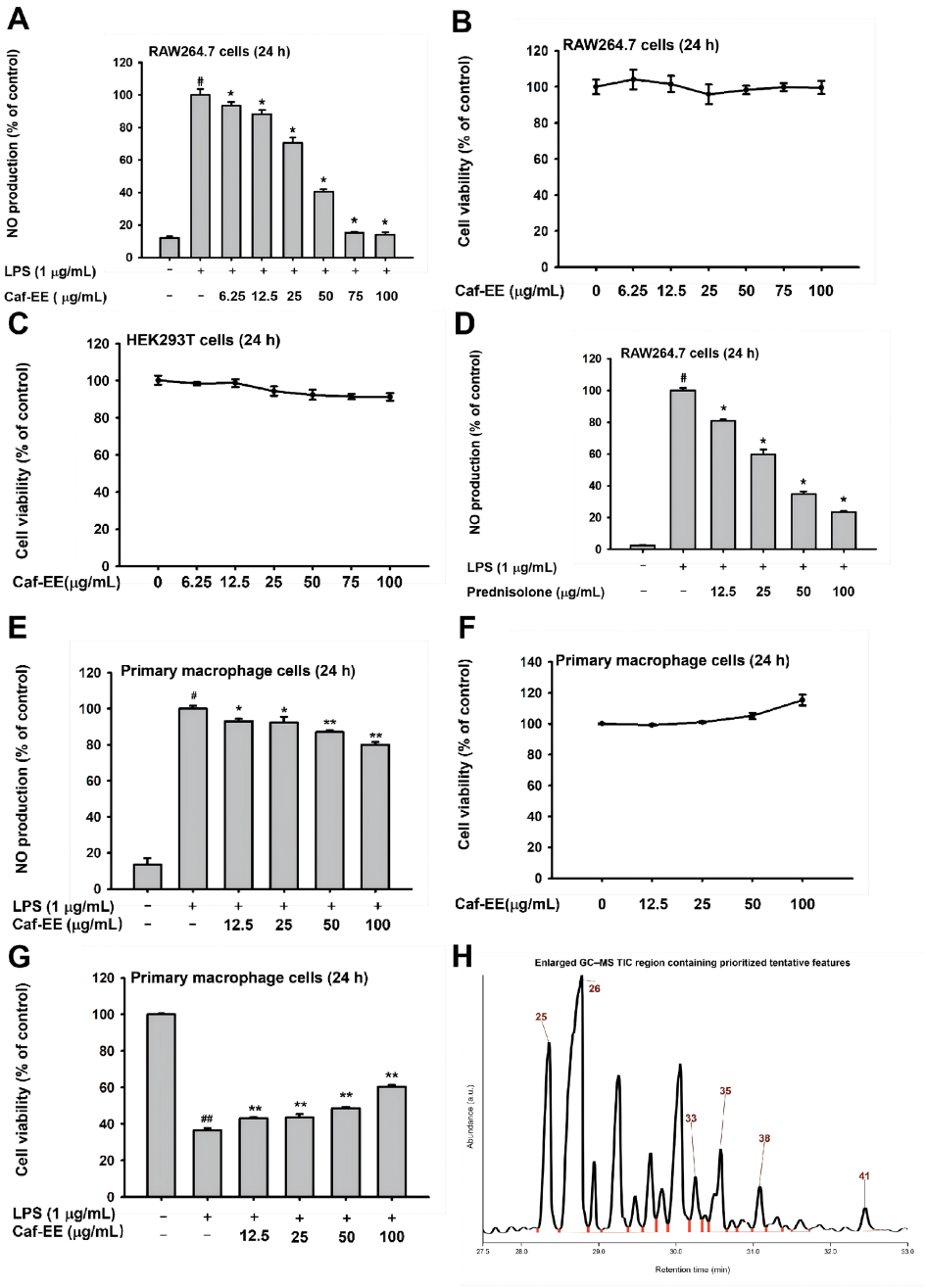

Fig. 1. Anti-inflammatory activity of Caf-EE and GC–MS-based characterization of its chemical features. (A) Effect of Caf-EE on nitrite production in LPS-stimulated RAW264.7 cells after 24 h. (B) Effect of Caf-EE on the viability of RAW264.7 cells after 24 h. (C) Effect of Caf-EE on the viability of HEK293T cells after 24 h. (D) Inhibitory effect of prednisolone (12.5–100 μg/mL) on LPS-induced nitrite production in RAW264.7 cells. (E) Effect of Caf-EE on nitrite production in LPS-stimulated primary peritoneal macrophages. (F) Effect of Caf-EE on the viability of primary peritoneal macrophages. (G) Effect of Caf-EE on LPS-induced cytotoxicity in primary peritoneal macrophages. (H) Enlarged view of the GC–MS total-ion chromatogram showing the 27.5–33.0 min retention-time region. Six representative peaks (peak Nos. 25, 26, 33, 35, 38, and 41) are indicated in the chromatogram. The corresponding tentative library-matched annotations are summarized in Table 2. The full-range chromatogram is provided in **Supplementary Fig. 1**. The complete list of tentatively annotated GC–MS features is provided in **Supplementary Table 1**. These annotations were not confirmed using authentic reference standards or orthogonal chromatographic methods. Data in panels (A–G) are presented as mean ± SD from three independent experiments. #$p < 0.05$ and ##$p < 0.01$ versus the relevant unstimulated control group; *$p < 0.05$ and **$p < 0.01$ versus the relevant LPS-stimulated reference group; one-way ANOVA with Tukey post hoc testing. Caf-EE, *C. africana* ethanol extract; LPS, lipopolysaccharide; GC–MS, gas chromatography–mass spectrometry.

Table 2. Representative tentative GC–MS annotations from Caf-EE.

Peak No.	RT (min)	Relative peak area (% TIC)	Representative tentative annotation	CAS No.	NIST match quality	Downstream use/comment
25	28.351	10.269	Lanosta-8,24-dien-3-one	5539-04-8	90	Target prediction and exploratory docking
26	28.764	26.496	Lanost-8-en-7-one	52474-71-2	78	Target prediction and exploratory docking
33	30.247	2.698	9,19-Cyclolanost-24-en-3-ol	469-38-5	99	Target prediction and exploratory docking
35	30.573	4.787	Glutinol	545-24-4	99	Target prediction and exploratory docking
38	31.079	2.124	9,19-Cyclolanostan-3-ol, 24-methylene-, (3β)-	1449-09-8	90	Target prediction only; not included in the main docking analysis
41	32.441	1.279	Lanost-8-ene-3,7-dione	55401-48-4	76	Target prediction only; not included in the main docking analysis

Note: The listed entries are tentative GC–MS library annotations. Relative peak area is the percentage of total ion chromatogram peak area and does not indicate absolute concentration. Identities were not confirmed with authentic standards or orthogonal chromatographic methods. RT, retention time; TIC, total ion chromatogram; NIST, National Institute of Standards and Technology.

get network (Fig. 2B). GO biological process and KEGG pathway enrichment analyses revealed significant enrichment of inflammatory response, response to lipopolysaccharide, regulation of the MAPK cascade, and Toll-like receptor, NF-κB, MAPK, and TNF signaling pathways (Fig. 2C,D). Collectively, these analyses indicated that the predicted targets of Caf-EE are enriched in LPS-responsive and inflammation-related signaling pathways, indicating its anti-inflammatory activity.

3.3 Caf-EE Inhibits NF-κB and AP-1 Transcriptional Activity and Inflammatory Gene Expression

To examine the effects of Caf-EE on NF-κB and AP-1 transcriptional activity, MyD88- and TRIF-induced luciferase activities were measured in HEK293T cells. Caf-EE significantly suppressed MyD88-mediated NF-κB transcriptional activity at all tested concentrations (50–100 μg/mL), whereas TRIF-mediated NF-κB transcriptional activity was significantly reduced at 75 and 100 μg/mL (Fig. 3A,B). A similar pattern was observed for AP-1, with Caf-EE suppressing MyD88-mediated transcriptional activity at 50–100 μg/mL and TRIF-mediated transcriptional activity only at 100 μg/mL (Fig. 3C,D). Consistent with the inhibition of NF-κB and AP-1 transcriptional activities, Caf-EE reduced the mRNA expression of *IL-1β* and *iNOS* in LPS-stimulated RAW264.7 cells (Fig. 3E). In addition, Caf-EE attenuated LPS-induced phosphorylation of p50 (60 min), p65 (5 and 60 min), and c-Jun (30 min), further supporting inhibition of NF-κB/AP-1 signaling (Fig. 3F).

3.4 Caf-EE Modulates Src- and TAK1-Mediated Inflammatory Signaling

Because Caf-EE suppressed MyD88- and TRIF-mediated NF-κB/AP-1 transcriptional activity, we next investigated upstream signaling molecules involved in these pathways. Src acts upstream of NF-κB signaling, whereas TAK1 regulates the MAPK/AP-1 signaling cascade [12,13,14]. Accordingly, the effects of Caf-EE on Src- and TAK1-associated signaling were investigated.

Caf-EE reduced the phosphorylation of Src and its downstream signaling molecules IKKα/β and IκBα during the early phase of LPS stimulation in RAW264.7 cells (Fig. 4A). Consistently, Caf-EE also inhibited the phosphorylation of overexpressed HA-Src in HEK293T cells (Fig. 4B). To further assess the effect of Caf-EE on Src kinase activity, ATP-dependent Src autophosphorylation was examined using immunoprecipitated HA-Src. Addition of ATP markedly increased autophosphorylation at Src Tyr416, whereas Caf-EE reduced Src autophosphorylation. The Src inhibitor PP2, used as a positive control, showed a similar inhibitory effect (**Supplementary Fig. 2**). Caf-EE also increased the thermal stability of Src in CETSA (Fig. 4C). Furthermore, Caf-EE reduced the phosphorylation of TAK1 and its downstream kinases MKK4/7 and JNK during the early time course following LPS stimulation, whereas p38 phosphorylation was unaffected (Fig. 4D). CETSA further showed that Caf-EE increased the thermal stability of TAK1 (Fig. 4E). Collectively, these findings suggest that Caf-EE modulates Src- and TAK1-mediated signaling pathways.

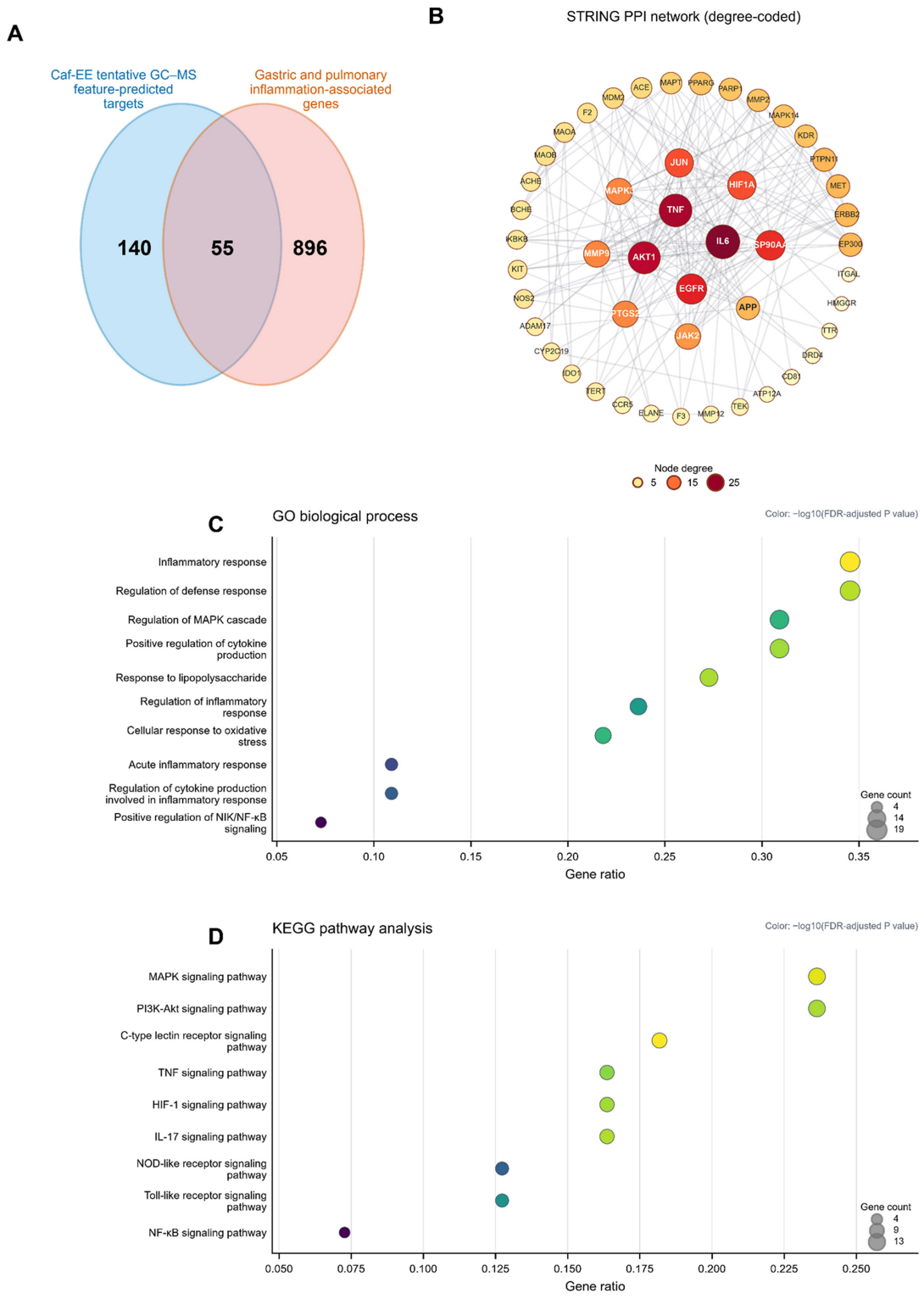

Fig. 2. Network pharmacology analysis of Caf-EE. (A) Identification of overlapping targets between predicted Caf-EE targets and gastric/pulmonary inflammation-associated genes. (B) Largest connected component of the Protein–protein interaction (PPI) network generated from the 55 overlapping targets using STRING (confidence score ≥0.700), comprising 47 targets; the smaller connected component and isolated targets are not shown. Node size and color indicate node degree, with larger and darker nodes indicating higher degrees of connectivity. (C) Gene Ontology (GO) biological process enrichment analysis of the overlapping targets. Dot size represents gene count, and dot color indicates –log10(FDR-adjusted *p* value). (D) Kyoto Encyclopedia of Genes and Genomes (KEGG) pathway enrichment analysis of the overlapping targets. Dot size represents gene count, and dot color indicates –log10(FDR-adjusted *p* value).

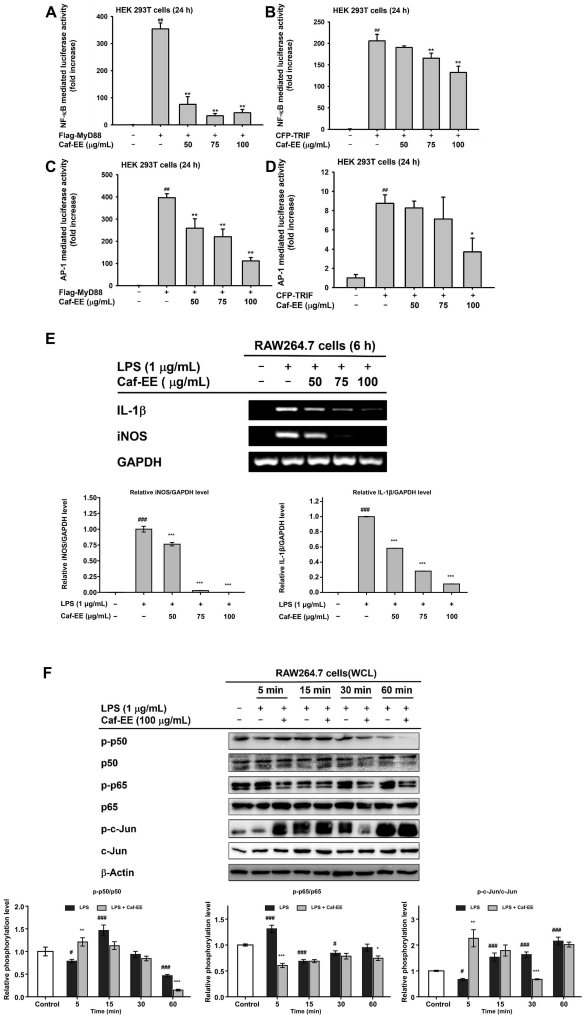

Fig. 3. Caf-EE suppresses NF-κB and AP-1 transcriptional activity and inflammatory gene expression. (A) Effect of Caf-EE (50, 75, and 100 μg/mL) on MyD88-mediated NF-κB transcriptional activity in HEK293T cells transfected with an NF-κB luciferase reporter, Flag-MyD88 or Flag empty vector, and β-gal plasmid. Firefly luciferase activity was normalized to β-gal activity. (B) Effect of Caf-EE (50, 75, and 100 μg/mL) on TRIF-mediated NF-κB transcriptional activity in HEK293T cells transfected with an NF-κB luciferase reporter, CFP-TRIF or CFP empty vector, and β-gal plasmid. Firefly luciferase activity was normalized to β-gal activity. (C) Effect of Caf-EE (50, 75, and 100 μg/mL) on MyD88-mediated AP-1 transcriptional activity in HEK293T cells transfected with an AP-1 luciferase reporter, Flag-MyD88 or Flag empty vector, and β-gal plasmid. Firefly luciferase activity was normalized to β-gal activity. (D) Effect of Caf-EE (50, 75, and 100 μg/mL) on TRIF-mediated AP-1 transcriptional activity in HEK293T cells transfected with an AP-1 luciferase reporter, CFP-TRIF or CFP empty vector, and β-gal plasmid. Firefly luciferase activity was normalized to β-gal activity. (E) Effects of Caf-EE (50, 75, and 100 μg/mL) on IL-1β and iNOS mRNA expression in RAW264.7 cells pretreated with Caf-EE for 30 min before stimulation with LPS (1 μg/mL) for 6 h. Band intensities were quantified as IL-1β/GAPDH and iNOS/GAPDH ratios and normalized to the LPS-treated group. (F) Effects of Caf-EE (100 μg/mL) on LPS-induced phosphorylation of p50, p65, and c-Jun in RAW264.7 cells pretreated with Caf-EE for 30 min before LPS stimulation for the indicated times. All data are presented as mean ± SD from three independent experiments. Statistical significance was assessed by one-way ANOVA followed by Tukey's multiple-comparisons test for panels (A–D). For panel (E), two separate one-way ANOVA analyses followed by Dunnett's multiple-comparisons test were performed: one comparing the LPS-treated group with the unstimulated control group and the other comparing each Caf-EE-treated group with the LPS-treated group. For panel (F), comparisons with the unstimulated control were assessed by one-way ANOVA followed by Dunnett's multiple-comparisons test, whereas time-matched comparisons between LPS and LPS + Caf-EE groups were assessed by two-way ANOVA with Šídák-adjusted multiple comparisons. #$p < 0.05$, ##$p < 0.01$, and ###$p < 0.001$ denote comparisons with the relevant control group; *$p < 0.05$, **$p < 0.01$, and ***$p < 0.001$ denote comparisons with the relevant stimulated group. AP-1, Activator protein 1; MyD88, Myeloid differentiation primary response 88; TRIF, TIR-domain-containing adapter-inducing IFN-β; iNOS, Inducible nitric oxide synthase; IL-1β, Interleukin-1 beta; CFP, cyan fluorescent protein.

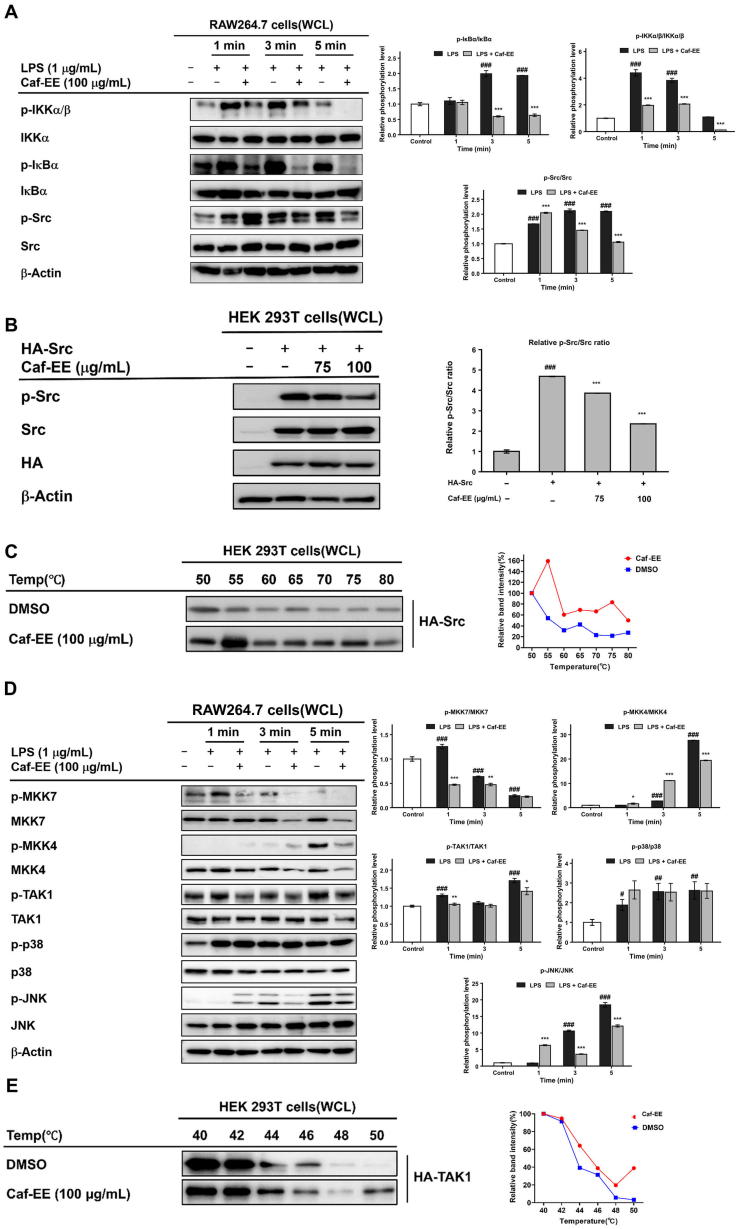

Fig. 4. Caf-EE regulates Src- and TAK1-associated signaling. (A) Representative immunoblots of p-IKKα/β, IKKα/β, p-IκBα, IκBα, p-Src, and Src in RAW264.7 cells pretreated with Caf-EE (100 μg/mL) for 30 min before LPS stimulation for the indicated times. Band intensities were quantified as p-IKKα/β/IKKα/β, p-IκBα/IκBα, and p-Src/Src ratios. (B) Representative immunoblots of p-Src, Src, HA, and β-actin in HA-Src-overexpressing HEK293T cells treated with Caf-EE (75 or 100 μg/mL). Band intensities were quantified as p-Src/Src ratios. (C) CETSA analysis of Src following Caf-EE treatment. (D) Representative immunoblots of p-MKK7, MKK7, p-MKK4, MKK4, p-TAK1, TAK1, p-p38, p38, p-JNK, and JNK in RAW264.7 cells. Band intensities were quantified as p-MKK7/MKK7, p-MKK4/MKK4, p-TAK1/TAK1, p-p38/p38, and p-JNK/JNK ratios. (E) CETSA analysis of TAK1 following Caf-EE treatment. For immunoblot quantification, phospho/total-protein ratios were normalized to the mean of the corresponding untreated control group, which was set to 1. Quantitative data in panels (A,B,D) are presented as mean ± SD from three independent experiments. In panels (A,D), LPS-stimulated groups were compared with the unstimulated control using one-way ANOVA followed by Dunnett's multiple-comparisons test, whereas LPS + Caf-EE groups were compared with the time-matched LPS groups using two-way ANOVA followed by Šídák-adjusted comparisons. In panel (B), statistical significance was assessed by one-way ANOVA followed by Dunnett's multiple-comparisons test against the HA-Src + vehicle group. #$p < 0.05$, ##$p < 0.01$, and ###$p < 0.001$ denote comparisons with the relevant control group; *$p < 0.05$, **$p < 0.01$, and ***$p < 0.001$ denote comparisons with the relevant stimulated or reference group. TAK1, Transforming growth factor-β-activated kinase 1; IKKα/β, IκB kinase alpha/beta; IκBα, Inhibitor of NF-κB alpha; MKK4, MAPK kinase 4; MKK7, MAPK kinase 7; CETSA, cellular thermal shift assay; JNK, c-Jun N-terminal kinase; HA, hemagglutinin.

Table 3. Predicted docking affinities of four representative tentative GC–MS features against Src and TAK1.

Tentative GC–MS feature	Target protein	Predicted affinity (kcal/mol)
Lanosta-8,24-dien-3-one/lanosterone	Src	–8.881
Lanosta-8,24-dien-3-one/lanosterone	TAK1	–7.992
Lanost-8-en-7-one	Src	–9.259
Lanost-8-en-7-one	TAK1	–8.142
Glutinol	Src	–8.485
Glutinol	TAK1	–8.005
9,19-Cyclolanost-24-en-3-ol	Src	–9.856
9,19-Cyclolanost-24-en-3-ol	TAK1	–8.257

Note: More negative values indicate lower predicted docking energy. Docking was interpreted as exploratory structural modeling and not as proof of direct binding or ATP-competitive inhibition.

3.5 Molecular Docking Analysis of Tentative GC–MS Annotations From Caf-EE Against Src and TAK1

Molecular docking analyses were performed using four tentative GC–MS annotations against Src and TAK1 (Fig. 5A). The selected tentative annotations included lanosta-8,24-dien-3-one, lanost-8-en-7-one, glutinol, and 9,19-cyclolanost-24-en-3-ol (Fig. 5B). All four tentatively annotated structures showed favorable predicted binding affinities toward Src and TAK1, with 9,19-cyclolanost-24-en-3-ol exhibiting the strongest predicted binding to both Src (–9.856 kcal/mol) and TAK1 (–8.257 kcal/mol) (Fig. 5C and Table 3). Predicted binding models of 9,19-cyclolanost-24-en-3-ol with Src and TAK1 suggested interactions with Src residues Leu273, Val281, Lys295, Met314, Thr338, Asp404, and Phe405, and with TAK1 residues Val50, Val90, Met104, Ala107, Ser111, Leu163, and Cys174 (Fig. 5D,E). These predicted contacts were predominantly hydrophobic, with limited possible near-polar interactions (**Supplementary Fig. 3**).

To validate the docking protocol, the co-crystallized ligands AMP-PNP and takinib were redocked into Src and TAK1, respectively, to assess whether their crystallographic binding poses could be reproduced. The top-ranked redocked poses showed symmetry-corrected heavy-atom RMSD values of 1.354 Å for Src and 0.447 Å for TAK1 relative to their respective crystallographic poses, both satisfying the ≤2.0 Å criterion (**Supplementary Table 2** and **Supplementary Fig. 4**).

3.6 Caf-EE Attenuates HCl/EtOH-Induced Acute Gastric Mucosal Injury

To evaluate the anti-inflammatory effects of Caf-EE *in vivo*, an HCl/EtOH-induced acute gastric mucosal injury model was employed [34,35]. HCl/EtOH induced extensive hemorrhagic gastric lesions, whereas Caf-EE significantly reduced the lesion area at 50 and 100 mg/kg, with the strongest protective effect observed at 100 mg/kg. Ranitidine, used as a positive control, also markedly reduced gastric lesion formation (Fig. 6A,B). In gastric tissues, neither Caf-EE nor ranitidine reduced *IL-1β* mRNA expression. In contrast, Caf-EE (100 mg/kg) reduced *IL-6* mRNA expression, whereas ranitidine increased *IL-6* expression (Fig. 6C). In addition, Caf-EE and ranitidine reduced the phosphorylation of Src and TAK1 in gastric tissues (Fig. 6D).

3.7 Caf-EE Ameliorates LPS-Induced Acute Lung Injury

To further evaluate the anti-inflammatory activity of Caf-EE *in vivo*, an LPS-induced acute lung injury model was employed. Histological analysis showed that LPS induced marked inflammatory cell infiltration and alveolar structural damage, whereas treatment with Caf-EE (50 and 100 mg/kg) or dexamethasone (positive control; 5 mg/kg) attenuated these pathological changes (Fig. 7A). Consistent with the histological findings, acute lung injury scores were significantly reduced by Caf-EE at both doses and by dexamethasone (Fig. 7B). Pulmonary edema, assessed by the lung wet-to-dry weight ratio, was significantly reduced only in the Caf-EE 100 mg/kg group, although all treatment groups showed a decreasing trend (Fig. 7C). In lung tissues, Caf-EE (100 mg/kg) significantly reduced the mRNA expression of both *TNF-α* and *IL-1β*, whereas dexamethasone significantly reduced *TNF-α* but not *IL-1β* expression (Fig. 7D). Furthermore, Caf-EE (100 mg/kg) reduced Src and TAK1 phosphorylation, whereas dexamethasone reduced Src phosphorylation but not TAK1 phosphorylation in lung tissues (Fig. 7E).

4. Discussion

The present study combined multiple experimental and computational approaches to investigate the anti-inflammatory activity of Caf-EE, including *in vitro* and *in vivo* inflammatory models, signaling analyses, network pharmacology, and molecular docking. This experimental framework is consistent with established concepts that inflammation coordinates protective host responses [36], TLRs, particularly TLR4, drive LPS-induced innate immune signaling [37,38], and nitric oxide/iNOS-derived nitrite is a major macrophage inflammatory readout [39,40]. This integrated approach provides mechanistic insight into

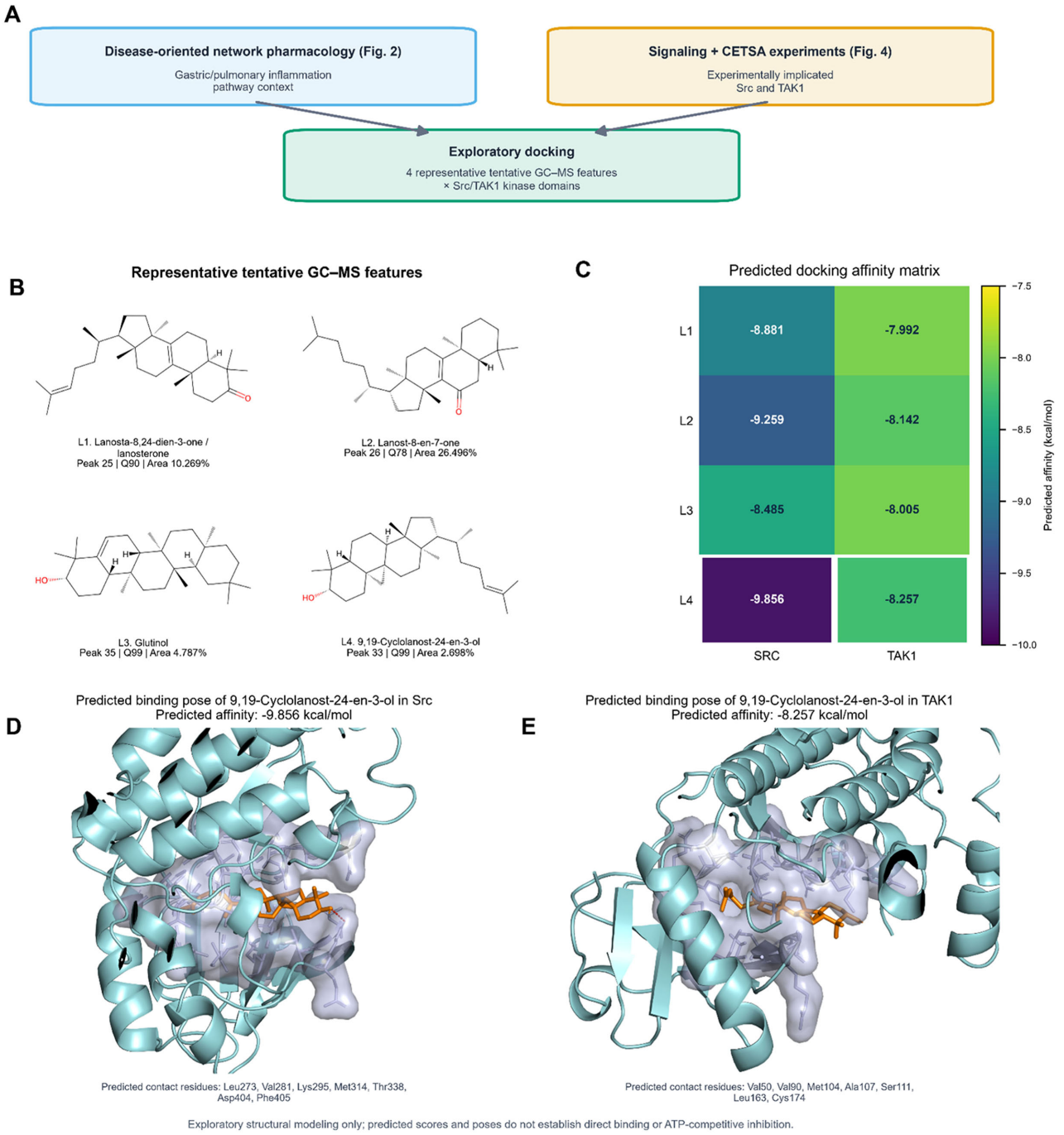

Fig. 5. Predicted interactions of tentative GC–MS annotations with Src and TAK1. (A) Workflow illustrating the molecular docking strategy. Tentative GC–MS annotations were selected from the GC–MS analysis, whereas Src and TAK1 were selected from the experimental signaling and CETSA analyses as docking targets. (B) Structure of four tentative GC–MS annotations selected for molecular docking analysis. (C) Predicted binding affinities of the four tentatively annotated structures toward Src and TAK1. More negative values indicate stronger predicted binding affinity. (D,E) Predicted binding models of 9,19-cyclolanost-24-en-3-ol with Src and TAK1, showing the predicted interacting residues.

the anti-inflammatory activity of Caf-EE while supporting the involvement of Src/TAK1-associated signaling.

Network pharmacology analyses demonstrated that the predicted targets of Caf-EE were significantly enriched in inflammation-related biological processes and signaling pathways, including inflammatory response, response to lipopolysaccharide, and TLR-, NF-κB-, MAPK-, and TNF-associated signaling pathways. These findings sug-

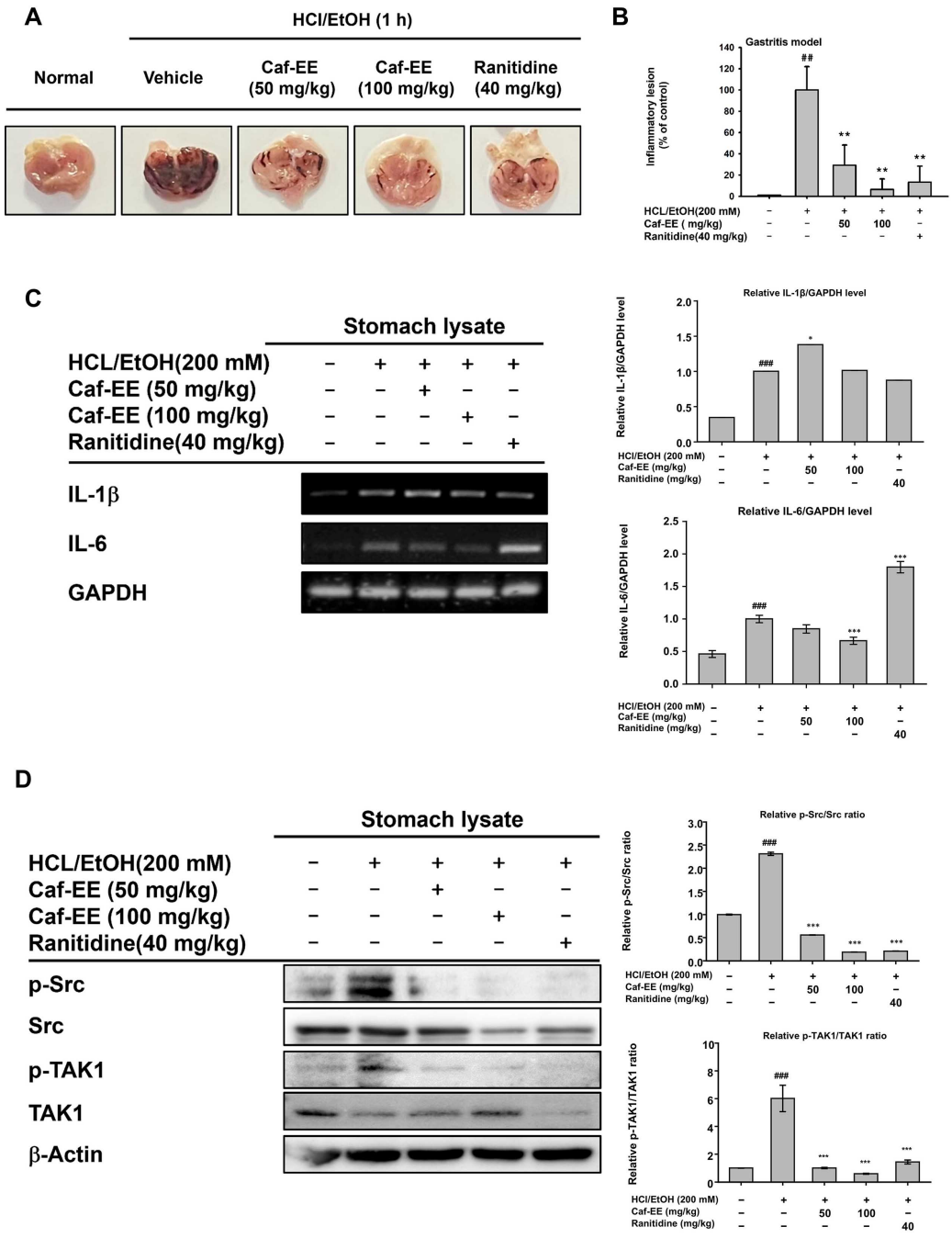

Fig. 6. Protective effects of Caf-EE in an HCl/EtOH-induced acute gastric injury model. (A) Representative gastric images from mice orally pretreated with vehicle, Caf-EE (50 or 100 mg/kg), or ranitidine (40 mg/kg) before induction of acute gastric mucosal injury by oral administration of 200 mM HCl in 60% ethanol. (B) Quantification of gastric lesion area, expressed as a percentage of the HCl/EtOH group, which was set to 100%. (C) Semi-quantitative RT-PCR analysis of IL-1β and IL-6 mRNA expression in gastric tissues. Band intensities were quantified as IL-1β/GAPDH and IL-6/GAPDH ratios and normalized to the HCl/EtOH-treated group. (D) Representative immunoblots for Src and TAK1 phosphorylation in gastric tissue lysates. Densitometric p-Src/Src and p-TAK1/TAK1 ratios were normalized to the mean of the normal group, which was set to 1. Data in panel (B) are presented as mean ± SD (n = 7 mice per group), whereas quantitative data in panels (C,D) are presented as mean ± SD from three randomly selected mice per group. Two separate one-way ANOVA analyses followed by Dunnett's multiple-comparisons test were performed: one comparing the HCl/EtOH-treated group with the normal control group and the other comparing each treatment group with the HCl/EtOH-treated group. ##$p < 0.01$ and ###$p < 0.001$ denote comparisons with the normal control group; *$p < 0.05$, **$p < 0.01$, and ***$p < 0.001$ versus the HCl/EtOH group.

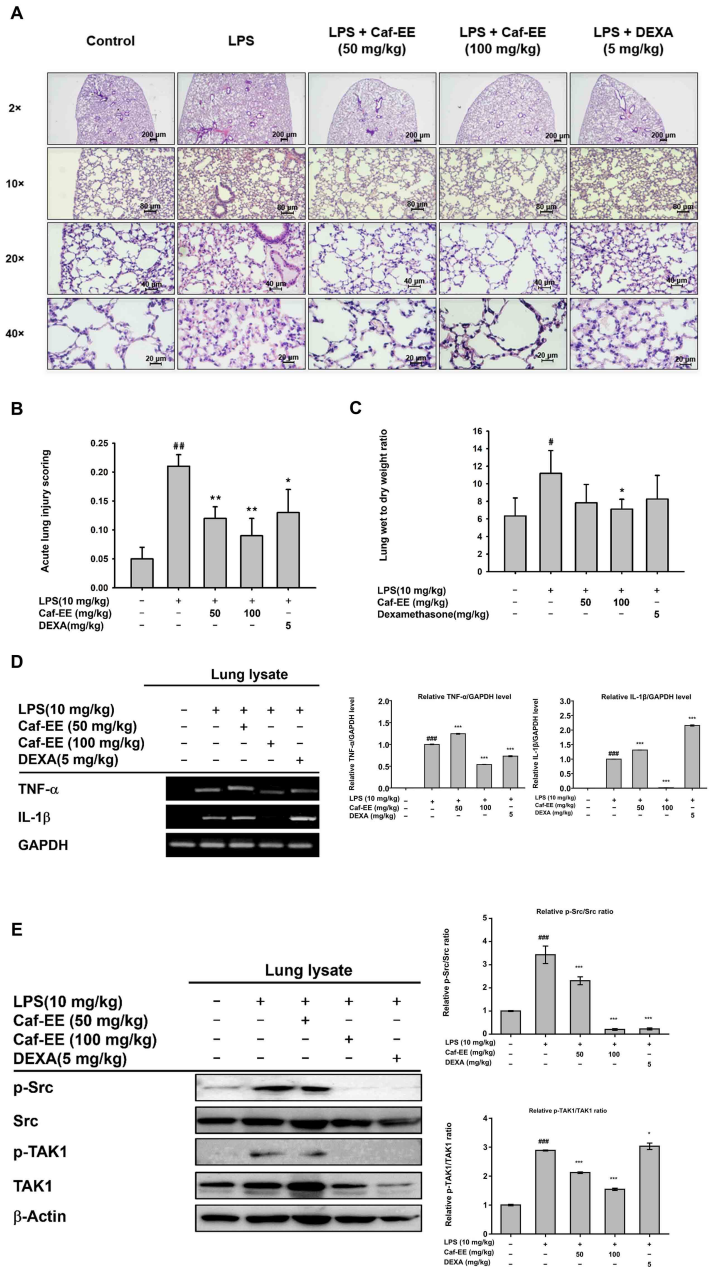

Fig. 7. Caf-EE attenuates LPS-induced acute lung injury. (A) Representative H&E-stained lung sections from control mice receiving vehicle and intranasal PBS, and from mice treated with vehicle, Caf-EE (50 or 100 mg/kg) or dexamethasone (5 mg/kg) and challenged intranasally with LPS to induce acute lung injury. Lung sections are shown at 2×, 10×, 20×, and 40× magnifications. Scale bars represent 200 μm, 80 μm, 40 μm, and 20 μm for the 2×, 10×, 20×, and 40× images, respectively. (B) Histological lung injury scores based on H&E-stained lung sections. (C) Lung wet-to-dry weight ratio. (D) Semi-quantitative RT-PCR analysis of TNF-α and IL-1β mRNA expression in lung tissues. Band intensities were quantified as TNF-α/GAPDH and IL-1β/GAPDH ratios and normalized to the LPS-treated group. (E) Representative immunoblots and densitometric analysis of Src and TAK1 phosphorylation in lung tissues. Densitometric p-Src/Src and p-TAK1/TAK1 ratios were normalized to the mean of the control group, which was set to 1. Data in panels (B,C) are presented as mean ± SD (n = 7 mice per group), whereas quantitative data in panels (D,E) are presented as mean ± SD from three randomly selected mice per group. Two separate one-way ANOVA analyses followed by Dunnett's multiple-comparisons test were performed: one comparing the LPS-treated group with the control group and the other comparing each treatment group with the LPS-treated group. #$p < 0.05$, ##$p < 0.01$ and ###$p < 0.001$ denote comparisons with the control group; *$p < 0.05$, **$p < 0.01$, and ***$p < 0.001$ denote comparisons with the LPS-treated group.

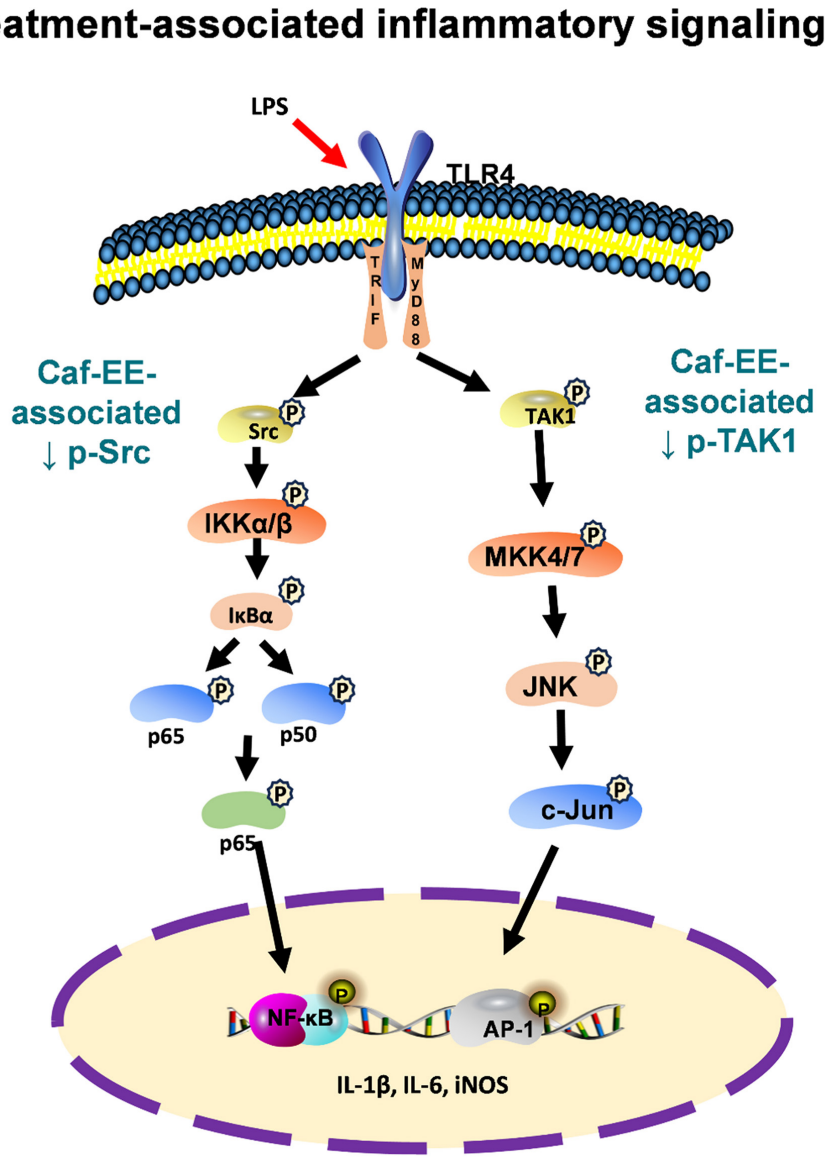

Fig. 8. Proposed mechanism underlying the anti-inflammatory activity of Caf-EE. Caf-EE modulates Src/TAK1-associated signaling, leading to reduced NF-κB/AP-1-dependent inflammatory responses. The green arrows indicate decreased phosphorylation associated with Caf-EE treatment.

gest that Caf-EE may modulate multiple inflammatory signaling pathways, providing a rationale for the subsequent mechanistic investigation. Because several of the enriched pathways converge on NF-κB- and AP-1-mediated inflammatory signaling, we next investigated these signaling cascades to elucidate the molecular mechanism underlying the anti-inflammatory activity of Caf-EE.

Mechanistically, Caf-EE reduced phosphorylation of both NF-κB- and AP-1-associated signaling molecules, including IKK/IκB, MKK4/7, JNK, and c-Jun. In addition, Caf-EE reduced the phosphorylation of Src and TAK1, which are established upstream regulators of the NF-κB and AP-1 signaling pathways [12,13,14,41]. Consistent with the reduced Src phosphorylation, Caf-EE reduced ATP-dependent Src autophosphorylation in an assay using immunoprecipitated HA-Src. However, because immunoprecipitated HA-Src is not a purified Src preparation and may contain other cellular proteins, this finding alone does not establish that Caf-EE directly inhibits Src catalytic activity. Nevertheless, the reduced Src autophosphorylation provides additional functional evidence supporting the modulation of Src-associated signaling by Caf-EE.

CETSA further provided supportive evidence for the involvement of Src and TAK1 in the activity of Caf-EE. Compared with the vehicle-treated groups, Caf-EE treatment produced distinct temperature-dependent changes in soluble Src and TAK1, including pronounced increases in soluble Src at 55 °C and soluble TAK1 at 50 °C. These find-

ings suggest that Caf-EE treatment alters the thermal stability profiles of Src and TAK1. Because ligand binding can stabilize proteins against thermal denaturation, these changes further support a potential interaction between components of Caf-EE and Src/TAK1 [32,33,42]. However, because CETSA measures changes in protein thermal stability rather than direct binding, and changes in thermal stability can arise from factors other than ligand binding, these observations should be interpreted as indirect evidence supporting an association with Src/TAK1-related signaling rather than proof of direct target engagement.

Interestingly, Caf-EE did not uniformly suppress all downstream targets of TAK1. Instead, Caf-EE preferentially suppressed the TAK1–MKK4/7–JNK signaling axis, whereas p38 phosphorylation remained largely unaffected. Although both kinases can be activated downstream of TAK1, accumulating evidence indicates that JNK and p38 are differentially regulated depending on the cellular context, activation kinetics, and phosphatase-mediated feedback mechanisms [10,43,44]. Therefore, the preferential inhibition of JNK by Caf-EE may reflect the distinct regulatory mechanisms governing individual MAPK branches downstream of TAK1.

Consistent with the observed modulation of Src/TAK1-associated signaling, Caf-EE inhibited both MyD88- and TRIF-mediated NF-κB/AP-1 transcriptional activity, although the inhibitory effect was consistently more pronounced under MyD88 overexpression. This finding may indicate that Caf-EE exerts a greater inhibitory effect on MyD88-dependent inflammatory signaling than on TRIF-dependent signaling under the present experimental conditions. This differential response may reflect differences in the molecular organization or activation mechanisms of the MyD88- and TRIF-dependent signaling pathways. Further studies will be required to determine the molecular basis underlying this differential response.

Previous studies provide broader evidence supporting the anti-inflammatory activity of the genus *Commiphora*. In an experimental arthritis model, a gum-guggul fraction from *Commiphora mukul* reduced joint swelling [45]. A crude *C. mukul* extract also downregulated inflammatory mediators and inhibited MAPK signaling in activated immune cells [46]. In *Commiphora myrrha*, ethanol extract and fractions reduced inflammation-related edema and prostaglandin E2 production, accompanied by analgesic activity [47]. Consistent with these observations, *C. africana* studies have likewise reported anti-inflammatory potential. Stem-leaf extracts inhibited cyclooxygenase-1/cyclooxygenase-2 (COX-1/COX-2) activity and reduced prostaglandin-related readouts *in vitro* [48], whereas a hydroethanolic stem-bark extract attenuated inflammation and pain endpoints in rodent models [49]. In addition, our findings suggest that Caf-EE exerts its anti-inflammatory effects, at least in part, through modulation of the Src/TAK1 signaling axis.

Among the representative tentative GC–MS-annotated compounds, 9,19-cyclolanost-24-en-3-ol showed the highest predicted affinity toward both Src and TAK1. Previous studies have demonstrated that structurally related cycloartane-type triterpenoids possess anti-inflammatory properties [50]. For example, a novel 9,19-cyclolanostane glycoside isolated from *Actaea vaginata* suppressed LPS-induced NO production, inhibited iNOS expression and pro-inflammatory cytokine production, and attenuated NF-κB activation in activated macrophages [51]. Similarly, cycloart-7-ene triterpenoid glycosides isolated from *Cimicifuga dahurica* inhibited NO production through downregulation of iNOS and COX-2 in LPS-stimulated RAW264.7 macrophages [52]. In addition, several cycloartane-type triterpenoids isolated from *C. dahurica* were reported to exhibit potent inhibitory effects on the production of IL-12p40, IL-6, and TNF-α in LPS-stimulated bone marrow-derived dendritic cells [53]. Together with our molecular docking analysis, these findings support the possibility that the putatively identified cycloartane-type triterpenoid 9,19-cyclolanost-24-en-3-ol may contribute, at least in part, to the anti-inflammatory activity of Caf-EE.

The chemical composition of a plant extract can influence its biological activities, and extraction conditions are important determinants of the chemical profile. Among these parameters, extraction temperature can affect both extraction efficiency and the composition of bioactive constituents [54]. Moderate temperatures may enhance solvent penetration, diffusion, and the release of phytochemicals from plant tissues, whereas excessive heat may promote degradation or chemical transformation of thermolabile constituents [54]. Therefore, although the temperature-dependent stability or recovery of individual compounds was not directly evaluated in this study, the extraction temperature was consistently controlled at 50 °C to promote reproducible preparation of Caf-EE and minimize potential variation in its chemical composition.

The anti-inflammatory effects of Caf-EE were further validated in two distinct acute inflammatory disease models. Because the HCl/EtOH-induced gastric injury model and the LPS-induced acute lung injury model differ substantially in the mode and temporal profile of injury induction, distinct dosing schedules were employed to appropriately evaluate the anti-inflammatory activity of Caf-EE in each model. Caf-EE alleviated gastric mucosal injury and LPS-induced acute lung injury, accompanied by reduced Src and TAK1 phosphorylation in both tissues, supporting the *in vivo* relevance of the Src/TAK1-associated signaling changes identified in macrophages.

In the lung injury model, both 50 and 100 mg/kg Caf-EE reduced Src and TAK1 phosphorylation, although the reductions were more pronounced at 100 mg/kg. This observation suggests that the magnitude of Src/TAK1-associated signaling modulation may vary with the adminis-

tered dose. However, because only two Caf-EE doses were evaluated, these findings are insufficient to establish a formal dose–response relationship.

Caf-EE also reduced inflammatory cytokine expression in LPS-driven *in vivo* models (Fig. 8). However, IL-1β mRNA was not reduced in the HCl/EtOH-induced gastric injury model. Similarly, although dexamethasone reduced Src phosphorylation in the LPS-induced acute lung injury model, its effects on inflammatory cytokine expression were not uniform, with a significant reduction in TNF-α but not IL-1β mRNA expression. Together, these findings suggest that modulation of Src/TAK1 signaling alone may not fully explain inflammatory cytokine expression across different inflammatory conditions. Further studies will be required to define the contribution of Src/TAK1-associated signaling relative to other regulatory pathways governing inflammatory cytokine expression.

5. Limitations

Several limitations of this study should be acknowledged. First, the chemical constituents of Caf-EE were only tentatively annotated by GC–MS library matching, with variable match quality among the selected features, and were not authenticated using reference standards or orthogonal chromatographic methods. Therefore, the bioactive constituents responsible for the anti-inflammatory activity of Caf-EE remain to be identified, and the downstream computational analyses based on these tentative annotations should be interpreted as hypothesis-generating.

Second, although phosphorylation analyses, CETSA, and molecular docking collectively support the proposed involvement of Src/TAK1-associated signaling, these approaches do not establish direct molecular interactions or direct target engagement. In addition, the differential regulation of inflammatory cytokines observed across experimental models suggests that Src/TAK1-associated signaling alone may not fully account for the anti-inflammatory activity of Caf-EE. Future studies incorporating target-specific positive controls, such as selective Src and TAK1 inhibitors, would provide additional validation of the proposed signaling mechanism and help define the contribution of Src/TAK1-associated signaling relative to other inflammatory regulatory pathways.

In addition to these mechanistic studies, future studies should focus on the isolation and characterization of active constituents, quantitative phytochemical analysis, and validation of direct molecular targets to further elucidate the bioactive components and molecular mechanisms underlying the anti-inflammatory activity of Caf-EE. Despite these limitations, the present study provides mechanistic evidence supporting the anti-inflammatory potential of Caf-EE and establishes a foundation for future phytochemical characterization, target-validation, and mechanism-guided natural product development.

6. Conclusions

In conclusion, Caf-EE exhibited anti-inflammatory activity in macrophages and two acute inflammatory disease models, accompanied by modulation of Src/TAK1-associated signaling and downstream NF-κB/AP-1-dependent inflammatory responses. These findings provide mechanistic support for the anti-inflammatory potential of *C. africana* and establish a scientific basis for its further investigation as a natural-source therapeutic candidate for inflammatory diseases. Future studies focusing on active constituent identification and target validation will facilitate the development of *C. africana*-derived anti-inflammatory agents.

Abbreviations

MTT, 3-(4,5-Dimethylthiazol-2-yl)-2,5-diphenyltetrazolium bromide; Caf-EE, *Commiphora africana* ethanol extract; FBS, Fetal bovine serum; TLR, Toll-like receptor; LPS, Lipopolysaccharide; MyD88, Myeloid differentiation primary response 88; Mal, MyD88-adaptor-like protein; TRIF, TIR-domain-containing adapter-inducing IFN-β; TRAM, TRIF-related adaptor molecule; NF-κB, Nuclear factor kappa B; AKT, Protein kinase B; IKKα/β, IκB kinase alpha/beta; IκBα, Inhibitor of NF-κB alpha; AP-1, Activator protein 1; TAK1, Transforming growth factor-β-activated kinase 1; JNK, c-Jun N-terminal kinase; MAPK, Mitogen-activated protein kinase; MKK4, MAPK kinase 4; MKK7, MAPK kinase 7; CETSA, Cellular thermal shift assay; iNOS, Inducible nitric oxide synthase; IL-1β, Interleukin-1 beta; IL-6, Interleukin-6; TNF-α, Tumor necrosis factor-alpha; DMSO, Dimethyl sulfoxide.

Availability of Data and Materials

The data supporting the findings of this study are included in the article and its supplementary materials. Additional raw data are available from the corresponding authors upon reasonable request.

Author Contributions

CM and JYC conceptualized the study. CM developed the methodology. JL and JHK performed validation. CM, LH, BHL, WYB and HWB conducted formal analysis. CM, YW, WC, BHL, WYB and HWB carried out investigation. JHK curated the data. CM, YW, and LH wrote the original draft. JL, JHK, and JYC reviewed and edited the manuscript. CM, YW, LH, JS, LY, ZH, YH, and WW contributed to visualization. JYC supervised the study, administered the project, and acquired funding. All authors read and approved the final manuscript. All authors contributed to editorial changes in the manuscript. All authors have participated sufficiently in the work and agreed to be accountable for all aspects of the work.

Ethics Approval and Consent to Participate

All animal procedures were approved by the Institutional Animal Care and Use Committee of Sungkyunkwan University (protocol no. SKKUIACUC2024-07-02-1). Animal experiments were performed in accordance with institutional guidelines and the National Institutes of Health (NIH) Guide for the care and use of laboratory animals. This study is reported in accordance with the ARRIVE 2.0 guidelines.

Acknowledgment

The authors thank the Sungkyunkwan University Core Facility for technical support with GC–MS analysis. The authors also thank Dr. Julius Dotto Keyyu and Dr. Bukombe John Kija for their contributions to the selection and botanical identification of *Commiphora africana* used in this study.

Funding

This research was funded by the National Research Foundation of Korea (NRF) through the Ministry of Education (Grant No. 2017R1A6A1A03015642) and the National Institute of Biological Resources (NIBR) (Grant Nos. NIBR202307203 and NIBR202606103).

Conflicts of Interest

The authors declare no conflicts of interest.

Declaration of AI and AI-Assisted Technologies in the Writing Process

During manuscript preparation, AI-assisted tools were used for language editing and consistency checking. The authors reviewed and edited all resulting text and take full responsibility for the scientific content and final manuscript.

Supplementary Material

Supplementary material associated with this article can be found, in the online version, at https://doi.org/10.31083/FBL55796.

References

[1] Furman D, Campisi J, Verdin E, Carrera-Bastos P, Targ S, Franceschi C, et al. Chronic inflammation in the etiology of disease across the life span. Nature Medicine. 2019; 25: 1822–1832. https://doi.org/10.1038/s41591-019-0675-0

[2] Medzhitov R. The spectrum of inflammatory responses. Science (New York, N.Y.). 2021; 374: 1070–1075. https://doi.org/10.1126/science.abi5200

[3] Fitzgerald KA, Kagan JC. Toll-like Receptors and the Control of Immunity. Cell. 2020; 180: 1044–1066. https://doi.org/10.1016/j.cell.2020.02.041

[4] Li D, Wu M. Pattern recognition receptors in health and diseases. Signal Transduction and Targeted Therapy. 2021; 6: 291. https://doi.org/10.1038/s41392-021-00687-0

[5] Gong T, Liu L, Jiang W, Zhou R. DAMP-sensing receptors in sterile inflammation and inflammatory diseases. Nature Reviews. Immunology. 2020; 20: 95–112. https://doi.org/10.1038/s41577-019-0215-7

[6] Duan T, Du Y, Xing C, Wang HY, Wang RF. Toll-Like Receptor Signaling and Its Role in Cell-Mediated Immunity. Frontiers in Immunology. 2022; 13: 812774. https://doi.org/10.3389/fimmu.2022.812774

[7] O'Neill LAJ, Bowie AG. The family of five: TIR-domain-containing adaptors in Toll-like receptor signalling. Nature Reviews. Immunology. 2007; 7: 353–364. https://doi.org/10.1038/nri2079

[8] Fitzgerald KA, Rowe DC, Barnes BJ, Caffrey DR, Visintin A, Latz E, et al. LPS-TLR4 signaling to IRF-3/7 and NF-kappaB involves the toll adapters TRAM and TRIF. The Journal of Experimental Medicine. 2003; 198: 1043–1055. https://doi.org/10.1084/jem.20031023

[9] Liu T, Zhang L, Joo D, Sun SC. NF-κB signaling in inflammation. Signal Transduction and Targeted Therapy. 2017; 2: 17023. https://doi.org/10.1038/sigtrans.2017.23

[10] Arthur JSC, Ley SC. Mitogen-activated protein kinases in innate immunity. Nature Reviews. Immunology. 2013; 13: 679–692. https://doi.org/10.1038/nri3495

[11] Lawrence T. The nuclear factor NF-kappaB pathway in inflammation. Cold Spring Harbor Perspectives in Biology. 2009; 1: a001651. https://doi.org/10.1101/cshperspect.a001651

[12] Lee CY, Kim HG, Park SH, Jang SG, Park KJ, Kim DS, et al. Anti-Inflammatory Functions of Alverine via Targeting Src in the NF-κB Pathway. Biomolecules. 2020; 10: 611. https://doi.org/10.3390/biom10040611

[13] Byeon SE, Yi YS, Oh J, Yoo BC, Hong S, Cho JY. The role of Src kinase in macrophage-mediated inflammatory responses. Mediators of Inflammation. 2012; 2012: 512926. https://doi.org/10.1155/2012/512926

[14] Ajibade AA, Wang HY, Wang RF. Cell type-specific function of TAK1 in innate immune signaling. Trends in Immunology. 2013; 34: 307–316. https://doi.org/10.1016/j.it.2013.03.007

[15] Ricciotti E, FitzGerald GA. Prostaglandins and inflammation. Arteriosclerosis, Thrombosis, and Vascular Biology. 2011; 31: 986–1000. https://doi.org/10.1161/ATVBAHA.110.207449

[16] Vane JR, Botting RM. Mechanism of action of nonsteroidal anti-inflammatory drugs. The American Journal of Medicine. 1998; 104: 2S–8S. https://doi.org/10.1016/s0002-9343(97)00203-9

[17] Bjarnason I, Scarpignato C, Holmgren E, Olszewski M, Rainsford KD, Lanas A. Mechanisms of Damage to the Gastrointestinal Tract From Nonsteroidal Anti-Inflammatory Drugs. Gastroenterology. 2018; 154: 500–514. https://doi.org/10.1053/j.gastro.2017.10.049

[18] Yang Y, Sun X, Peng C, Wei J, Yang X. The Genus Commiphora: An Overview of Its Traditional Uses, Phytochemistry, Pharmacology, and Quality Control. Pharmaceuticals (Basel, Switzerland). 2024; 17: 1524. https://doi.org/10.3390/ph17111524

[19] Kweyamba PA, Zofou D, Efange N, Assob JCN, Kitau J, Nyindo M. In vitro and in vivo studies on anti-malarial activity of Commiphora africana and Dichrostachys cinerea used by the Maasai in Arusha region, Tanzania. Malaria Journal. 2019; 18: 119. https://doi.org/10.1186/s12936-019-2752-8

[20] Segun PA, Ogbole OO, Ismail FMD, Nahar L, Evans AR, Ajaiyeoba EO, et al. Resveratrol derivatives from Commiphora africana (A. Rich.) Endl. display cytotoxicity and selectivity against several human cancer cell lines. Phytotherapy Research: PTR. 2019; 33: 159–166. https://doi.org/10.1002/ptr.6209

[21] Okumu M, Mbaria J, Gikunju J, Mbuthia P, Madadi V, Ochola F. Exploring nature's antidote: unveiling the inhibitory potential of selected medicinal plants from Kisumu, Kenya against venom from some snakes of medical significance in sub-Saharan

Africa. Frontiers in Pharmacology. 2024; 15: 1369768. https://doi.org/10.3389/fphar.2024.1369768
[22] Wang Y, Mou C, Huang L, Su J, You L, Zhang J, et al. The ethanolic extract of Rhaphidophora peepla prevents inflammation by inhibiting the activation of Syk/AKT/NF-κB and TAK1/MAPK/AP-1. Phytomedicine: International Journal of Phytotherapy and Phytopharmacology. 2025; 136: 156339. https://doi.org/10.1016/j.phymed.2024.156339
[23] Wang Y, Cho JY, Kim D. 20(S)-Protopanaxatriol alleviates gastritis by attenuating oxidative stress and inflammatory responses via inhibition of PI3K/AKT and JAK/STAT3 pathways. Journal of Ginseng Research. 2026; 50: 101062. https://doi.org/10.1016/j.jgr.2026.101062
[24] Jeon CM, Shin IS, Shin NR, Hong JM, Kwon OK, Kim JH, et al. Clausena anisata-mediated protection against lipopolysaccharide-induced acute lung injury in mice. International Journal of Molecular Medicine. 2016; 37: 1091–1098. https://doi.org/10.3892/ijmm.2016.2515
[25] Daina A, Michielin O, Zoete V. SwissTargetPrediction: updated data and new features for efficient prediction of protein targets of small molecules. Nucleic Acids Research. 2019; 47: W357–W364. https://doi.org/10.1093/nar/gkz382
[26] Rouillard AD, Gundersen GW, Fernandez NF, Wang Z, Monteiro CD, McDermott MG, et al. The harmonizome: a collection of processed datasets gathered to serve and mine knowledge about genes and proteins. Database: the Journal of Biological Databases and Curation. 2016; 2016: baw100. https://doi.org/10.1093/database/baw100
[27] Pletscher-Frankild S, Pallejà A, Tsafou K, Binder JX, Jensen LJ. DISEASES: text mining and data integration of disease-gene associations. Methods (San Diego, Calif.). 2015; 74: 83–89. https://doi.org/10.1016/j.ymeth.2014.11.020
[28] Szklarczyk D, Kirsch R, Koutrouli M, Nastou K, Mehryary F, Hachilif R, et al. The STRING database in 2023: protein-protein association networks and functional enrichment analyses for any sequenced genome of interest. Nucleic Acids Research. 2023; 51: D638–D646. https://doi.org/10.1093/nar/gkac1000
[29] Shannon P, Markiel A, Ozier O, Baliga NS, Wang JT, Ramage D, et al. Cytoscape: a software environment for integrated models of biomolecular interaction networks. Genome Research. 2003; 13: 2498–2504. https://doi.org/10.1101/gr.1239303
[30] Eberhardt J, Santos-Martins D, Tillack AF, Forli S. AutoDock Vina 1.2.0: New Docking Methods, Expanded Force Field, and Python Bindings. Journal of Chemical Information and Modeling. 2021; 61: 3891–3898. https://doi.org/10.1021/acs.jcim.1c00203
[31] Chen H, Hong YH, Woo BY, Hong YD, Manilack P, Souladeth P, et al. Cocculus hirsutus ameliorates gastric and lung injuries by suppressing Src/Syk. Phytomedicine: International Journal of Phytotherapy and Phytopharmacology. 2021; 93: 153778. https://doi.org/10.1016/j.phymed.2021.153778
[32] Martinez Molina D, Jafari R, Ignatushchenko M, Seki T, Larsson EA, Dan C, et al. Monitoring drug target engagement in cells and tissues using the cellular thermal shift assay. Science (New York, N.Y.). 2013; 341: 84–87. https://doi.org/10.1126/science.1233606
[33] Jafari R, Almqvist H, Axelsson H, Ignatushchenko M, Lundbäck T, Nordlund P, et al. The cellular thermal shift assay for evaluating drug target interactions in cells. Nature Protocols. 2014; 9: 2100–2122. https://doi.org/10.1038/nprot.2014.138
[34] Yuan Y, Wang X, Wang Y, Liu Y, Zhao L, Zhao L, et al. The Gastroprotective Effect of Walnut Peptides: Mechanisms and Impact on Ethanol-Induced Acute Gastric Mucosal Injury in Mice. Nutrients. 2023; 15: 4866. https://doi.org/10.3390/nu15234866
[35] Liu J, Lin H, Yuan L, Wang D, Wang C, Sun J, et al. Protective Effects of Anwulignan against HCl/Ethanol-Induced Acute Gastric Ulcer in Mice. Evidence-based Complementary and Alternative Medicine: ECAM. 2021; 2021: 9998982. https://doi.org/10.1155/2021/9998982
[36] Medzhitov R. Origin and physiological roles of inflammation. Nature. 2008; 454: 428–435. https://doi.org/10.1038/nature07201
[37] Kawai T, Akira S. The role of pattern-recognition receptors in innate immunity: update on Toll-like receptors. Nature Immunology. 2010; 11: 373–384. https://doi.org/10.1038/ni.1863
[38] Poltorak A, He X, Smirnova I, Liu MY, Van Huffel C, Du X, et al. Defective LPS signaling in C3H/HeJ and C57BL/10ScCr mice: mutations in Tlr4 gene. Science (New York, N.Y.). 1998; 282: 2085–2088. https://doi.org/10.1126/science.282.5396.2085
[39] Bogdan C. Nitric oxide and the immune response. Nature Immunology. 2001; 2: 907–916. https://doi.org/10.1038/ni1001-907
[40] Förstermann U, Sessa WC. Nitric oxide synthases: regulation and function. European Heart Journal. 2012; 33: 829–837. https://doi.org/10.1093/eurheartj/ehr304
[41] Benedik NS, Proj M, Steinebach C, Sova M, Sosič I. Targeting TAK1: Evolution of inhibitors, challenges, and future directions. Pharmacology & Therapeutics. 2025; 267: 108810. https://doi.org/10.1016/j.pharmthera.2025.108810
[42] Tu Y, Tan L, Tao H, Li Y, Liu H. CETSA and thermal proteome profiling strategies for target identification and drug discovery of natural products. Phytomedicine: International Journal of Phytotherapy and Phytopharmacology. 2023; 116: 154862. https://doi.org/10.1016/j.phymed.2023.154862
[43] Seternes OM, Kidger AM, Keyse SM. Dual-specificity MAP kinase phosphatases in health and disease. Biochimica et Biophysica Acta (BBA)-Molecular Cell Research. 2019; 1866: 124–143. https://doi.org/10.1016/j.bbamcr.2018.09.002
[44] Canovas B, Nebreda AR. Diversity and versatility of p38 kinase signalling in health and disease. Nature Reviews. Molecular Cell Biology. 2021; 22: 346–366. https://doi.org/10.1038/s41580-020-00322-w
[45] Sharma JN, Sharma JN. Comparison of the anti-inflammatory activity of Commiphora mukul (an indigenous drug) with those of phenylbutazone and ibuprofen in experimental arthritis induced by mycobacterial adjuvant. Arzneimittel-Forschung. 1977; 27: 1455–1457.
[46] Manjula N, Gayathri B, Vinaykumar KS, Shankernarayanan NP, Vishwakarma RA, Balakrishnan A. Inhibition of MAP kinases by crude extract and pure compound isolated from Commiphora mukul leads to down regulation of TNF-alpha, IL-1beta and IL-2. International Immunopharmacology. 2006; 6: 122–132. https://doi.org/10.1016/j.intimp.2005.07.001
[47] Su S, Wang T, Duan JA, Zhou W, Hua YQ, Tang YP, et al. Anti-inflammatory and analgesic activity of different extracts of Commiphora myrrha. Journal of Ethnopharmacology. 2011; 134: 251–258. https://doi.org/10.1016/j.jep.2010.12.003
[48] Compaoré M, Meda RNT, Bakasso S, Vlase L, Kiendrebeogo M. Antioxidative, anti-inflammatory potentials and phytochemical profile of Commiphora africana (A. Rich.) Engl. (Burseraceae) and Loeseneriella africana (Willd.) (Celastraceae) stem leaves extracts. Asian Pacific Journal of Tropical Biomedicine. 2016; 6: 665–670. https://doi.org/10.1016/j.apjtb.2016.06.001
[49] Ezekiel I, Mabrouk MA, Ayo JO. Study of the Effect of Hydro-Ethanolic Extract of Commiphora africana (Stem-bark) on Inflammation and Pain in Rodents. Asian Journal of Medical Sciences. 2010; 2: 81–84.
[50] Wang C, Mu X, Sun J. Research progress of cycloartane triterpenoids and pharmacological activities. Archiv Der Pharmazie. 2025; 358: e2400923. https://doi.org/10.1002/ardp.202400923
[51] Fang ZJ, Zhang T, Chen SX, Wang YL, Zhou CX, Mo

JX, et al. Cycloartane triterpenoids from Actaea vaginata with anti-inflammatory effects in LPS-stimulated RAW264.7 macrophages. Phytochemistry. 2019; 160: 1–10. https://doi.org/10.1016/j.phytochem.2019.01.003

[52] Pang QQ, Mei YD, Zhang YC, Liu LX, Shi DF, Pan DB, et al. Three new cycloart-7-ene triterpenoid glycosides from Cimicifuga dahurica and their anti-inflammatory effects. Natural Product Research. 2021; 35: 3634–3643. https://doi.org/10.1080/14786419.2020.1719487

[53] Thao NP, Lee YS, Luyen BTT, Oanh HV, Ali I, Arooj M, et al. Chemicals from Cimicifuga dahurica and Their Inhibitory Effects on Pro-inflammatory Cytokine Production by LPS-stimulated Bone Marrow-derived Dendritic Cells. Natural Product Sciences. 2018; 24: 194–198. https://doi.org/10.20307/nps.2018.24.3.194

[54] Sun S, Yu Y, Jo Y, Han JH, Xue Y, Cho M, et al. Impact of extraction techniques on phytochemical composition and bioactivity of natural product mixtures. Frontiers in Pharmacology. 2025; 16: 1615338. https://doi.org/10.3389/fphar.2025.1615338